Measurements of the Strong Coupling Constant and the QCD Colour Factors using Four-Jet Observables from Hadronic Z Decays in ALEPH[1]

Sílvia Bravo i Gallart
Universitat Autònoma de Barcelona
Departament de Física
Edifici Cn E-08193 Bellaterra (Barcelona)

September 2001

[1]Ph.D. Dissertation

Al meu padrí, perquè era com era.
Al Gon, perquè és com és.

The work presented in the following pages has provoked to me many and different feelings. But now, that all has finished, I will concentrate in the good ones.

Three years ago, in an ALEPH week, I met Dr. Günther Dissertori. He told to us, Hugo and myself, about a nice QCD analysis. Since Hugo was an anti-QCD guy (there is a "school" here at IFAE) there was no need to fight for it. Since then I have worked with and LEARNT FROM Günther, who became the supervisor of this thesis. Now I know I was very lucky to have the possibility to work with a QCD- "lover" and expert.

Of course, the possibility of writting such an "interesting" work is also due to IFAE, and more precisely to Dr. Enrique Fernández, who gave me the chance to enter the IFAE-community and the high energy physics environment.

From the IFAE-community I will first talk about Dra. Mª Lluïsa Mir. She has been almost always close to me (since some months she is living in the States), and I could explode and tell her what was making my days hard at any moment. Also Dra. Martine Bosman was close. I worked with her for my master thesis, which was a pleasure, but she kept showing interest for my work (and smiling!).

Before the death of the ALEPH experiment (*RIP*) there was an intense activity here at IFAE around the ALEPH data. A lot of meetings were held, and we were following and trying to help one to each other. To all the ALEPH meeting group (Lluïsa, Manel, Frederic, Aurelio, Imma, Pilar, Gon, Eugeni, Hugo and Javier) thanks a lot. I should mention also the ALEPH-CERN meeting group... they asked a lot, but helped also. Thanks to Günther, Roger, Hasko, John, etc. And to finish, some words to the BCAL team: Mokhtar, Pilar, Gon, Eugeni, Gaelle, Hugo, Javier and David. It was a pleasure to share with you the use of the portable phone!

Finally, I will not stop my "professional thanks giving" without talking about all the people I worked with when I discovered the particle physics world. I am talking about Martine, Matteo, Manuel and Irene.

Deixo l'anglès i vaig a la meva llengua materna: lo pontsicà. Cares i somriures ben variats m'han fet costat durant els dies - llargs, llarguíssims - que ha durat tot plegat. Ara mentre rumiava com escriure aquests agraïments pensava que sóc una persona afortunada, perquè tinc molts a qui agrair.

Tinc una família molt "maja", cadascú amb el seu tarannà, però tots ben "majos". Una "família adoptiva" que són una Perla (Negra). Una família que s'extén a partir del Gon i que he descobert molt gran, en extensió i en estima.

Les meves arrels pontsicanes es mantenen i s'engreixen amb els anys (a veure si aconsegueixo mantenir l'engreix a les arrels!). Els de ponent som guais, això no ho dubta ningú... ja ho diu la cançó "Ser de Lleida és lo millor que hi ha". Entre tota la tribu de ponent, a Ponts i comarca jo he conegut a gent molt gran. Em podria posar a dir noms i ompliria línies i més línies. Ho deixo aquí, dient-los gràcies a tots per estar aquí, o allí, o on esteu ara mateix.

En aquests dies de globalitzacions, immigracions i misèries una pobra pontsicana s'ha vist obligada a veure món... he conegut comarques noves, i finalment he deixat els meus "trastos" (de moment) a Castellar del Vallès. He vist que la gent de comarques, com ara els del barcelonès, són bona gent. Hi ha de tot, com a tot arreu, però jo m'he topat amb "de lo mejorcito, lo mejor". Els músics i les amants, físics en matrimoni i canalla, cerdanyolencs que es casen, que renten, que toquen, que juguen... un ventall de cares i maneres de fer digne d'estudi.

Aquí a l'IFAE he fet bons amics. Alguns encara hi són, altres han deixat les nostres parets verdes i han començat nova vida més lluny o més a prop. Tots són molt treballadors, i ves per on, en general molt barruts. N'hi ha de rinxolats, n'hi ha d'irisats, n'hi ha que fan punt de creu, n'hi ha que no es pentinen,...

Acabo amb música. La del Último de la fila, la dels Burros, la del Manolo García... la que m'ha acompanyat durant hores i hores, i que encapçala algunes seccions d'aquest treball.

I res, que fins aquí he arribat i a des d'aquí hauré de continuar. Espero tenir-vos al costat, a tots, durant molt i molt de temps.

GRÀCIES

Contents

List of Figures

List of Tables

Chapter 1

Introduction

It is generally believed that Quantum Chromodynamics (QCD) is the correct theory for the description of the strong interaction of quarks and gluons. This theory has been successfully tested at high energies, but proofs that QCD predicts some basic properties observed in nature, such as confinement of quarks in hadrons, are still missing. The lack of these proofs is due both to the mathematical complexity of the theory and to the non-applicability of the perturbative theory at low energies. Thanks to the enormous statistics accumulated at the LEP e^+e^- storage ring and the considerable theoretical progress in the field of perturbative QCD, the measurements and tests of QCD have entered the high precision regime. The strong coupling constant is not too "strong" at these high energies, which increases the reliability of perturbative calculations, and at the same time non-perturbative corrections to many observables, related to the hadronization of quarks and gluons into observable hadrons, become small.

During the last years, a large number of measurements have been performed and the theoretical predictions have been proved to predict better and better the experimental distributions. This improvement is due to new calculations that allow for an exact fixed order prediction at higher orders, but also to new Monte Carlo (MC) Programs. The latest versions of the already existing MCs as well as the new codes include the exact matrix elements for up to five-parton final state configurations. The present knowledge on the contributions of missing higher order terms and on soft phenomena, like hadronization, which cannot be described by the perturbative theory is also included.

The present thesis describes new measurements using LEP data collected by the ALEPH detector: first a measurement of the strong coupling constant alone, and then a

simultaneous measurement of the strong coupling constant and the colour factors, which represents a stringent test of QCD, will be presented in the following chapters. Such measurements have already been performed within the ALEPH collaboration, but new calculations and new Monte Carlo Programs have been available for some years now that allow for an improvement in the analysis.

The following chapters give the details of the measurements, and summarize the understanding on the performance of the new Monte Carlo programs. It all starts with an introduction to the theory of strong interactions, QCD, which can be found in Chapter 2. This is not intended to be a complete description of the theory, but tries to focus on the main concepts as well as on the more specific points which are important for the understanding of the measurement.

In the next chapter, the theoretical predictions for four-jet observables are detailed since these are the kind of observables used in the analyses of this thesis. It also includes the definition of the observables used.

Then, in Chapter 4 a description of the ALEPH detector is given. Once more, instead of an exhaustive discussion, only a brief description is given, with particular stress on the subdetectors or performances which are more relevant for the measurements presented in this work.

The next chapter contains a description of the analysis method. Details on the event selection, on the theoretical predictions and on the corrections used and on the fit procedure can be found there.

Chapter 6 gives all the details and results of the measurements. Plots of the corrections applied and of the fit results can be found there. First, the measurement of the strong coupling constant from the four-jet rate is presented. Then results on the simultaneous measurement of the strong coupling constant and the colour factors follow. Finally, a measurement to test the possible existence of a light gluino is shown.

Finally, before the conclusions, the studies performed with the new Monte Carlo pro-

grams used in the present thesis, which are not the standard for other ALEPH measurements, are described. Our present understanding of them and the limits to their applicability are discussed.

At the end of the present work an appendix summarizes the current discussions on one of the methods used for the measurement of the strong coupling constant from the four-jet rate: the experimentally optimized scale method.

Chapter 2

Theoretical framework

Jamás he podido respetar esas extrañas leyes.
Jamás lo podré disimular, luna vuela y hazme a mi volar.

2.1 Introduction

The theoretical description of hadron production in e^+e^- annihilation consists of four parts as shown in Fig. 2.1. The first part is based on the Standard Model of electroweak interactions [1]. Feynman diagrams are used to calculate the electroweak process of e^+e^- annihilation. The description of a multihadronic event starts with a pair of primary partons, quark-antiquark, distributed according to an exact (up to some order in α^{QED}) Z decay matrix element. The evolution of these primary partons under the strong interaction is described by perturbative Quantum Chromodynamics (pQCD). In a parton (or dipole) cascade, the primary partons evolve from the hard scattering scale $Q \approx \mathrm{M_Z}$ into secondary partons at a cut-off scale $Q_0 \approx 1\mathrm{GeV}$. It is during these calculable stages (hard subprocess and shower) that the event's global features are determined: energy dependences, event topologies, multiplicity, etc. In a third stage, carried out at the low virtuality scale Q_0, a model is employed to convert the secondary partons into hadrons. This hadronization process can modify the global properties of the event, but these modifications are small at the LEP energies. Finally the decay of unstable hadrons, which can be described by kinematics using experimentally measured decay rates, needs to be included before the prediction can be confronted with data.

While the standard model of particle physics provides a well tested description of the reaction $e^+e^- \to Z/\gamma^* \to q\bar{q}$, the subsequent production of observable hadrons is less well understood. The following sections try to summarize our current understanding of both

the evolution of partons under the strong interaction and the hadronization process. First, a short introduction to the Standard Model of particle physics is given. Then, a review of the perturbative theory of strong interactions is presented. Third, the problems of the non-perturbative regime, namely Soft QCD, are introduced. Finally, some details about the implementation of the current understanding of QCD in the Monte Carlo programs are given.

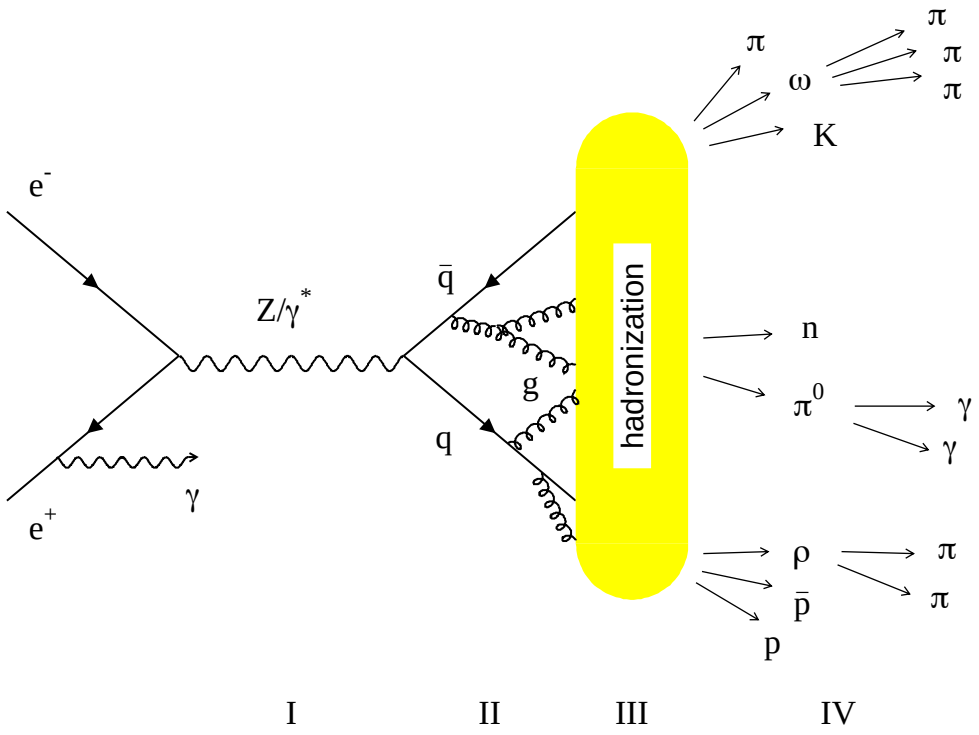

Figure 2.1: The reaction $e^+e^- \rightarrow hadrons$ viewed in four phases.

2.2 The Standard Model

A "standard model" is a theoretical framework, built from observations, which allows for predictions of physics phenomena. The Standard Model (SM) of particle physics [1, 2] provides a unified description of the electromagnetic, weak and strong forces in the language of quantum field theories. It has been experimentally verified with great accuracy over a wide range of energies and processes.

The SM is a quantum field gauge theory, based on the symmetry group $SU(3)_C \otimes SU(2)_L \otimes U(1)_Y$, partially characterized by the spectrum of elementary fields shown in Table 2.1. The matter fields are spin-$\frac{1}{2}$ fermions. There are three families of fermion fields, with similar properties except their masses, with the first family containing the constituents of stable matter: the up (u) and down (d) quarks (constituents of nucleons, as well as of pions and other mesons) and the electron (e) plus the electron-neutrino (ν_e). The quarks of the other two families are constituents of heavier short-lived particles. They and their companion charged leptons decay to the quarks and leptons of the first family via the weak force.

The interaction among fermions is mediated by spin-1 gauge bosons: one massless photon (γ) and eight massless gluons ($g_1, ..., g_8$) for the electromagnetic and strong interactions respectively, and three massive bosons ($W^{\pm}$ and Z) for the weak interaction.

Electrically charged particles interact due to the exchange of photons. The fact that the photon is massless accounts for the long range of the electromagnetic force.

Leptons

$$\begin{pmatrix} \nu_{e_L} \\ e_L \end{pmatrix}_{Y=-\frac{1}{2}} \quad \begin{pmatrix} \nu_{\mu_L} \\ \mu_L \end{pmatrix}_{Y=-\frac{1}{2}} \quad \begin{pmatrix} \nu_{\tau_L} \\ \tau_L \end{pmatrix}_{Y=-\frac{1}{2}}$$

$$\left(e_R\right)_{Y=-1} \quad \left(\mu_R\right)_{Y=-1} \quad \left(\tau_R\right)_{Y=-1}$$

Quarks

$$\begin{pmatrix} u_L \\ d'_L \end{pmatrix}_{Y=\frac{1}{6}} \quad \begin{pmatrix} c_L \\ s'_L \end{pmatrix}_{Y=\frac{1}{6}} \quad \begin{pmatrix} t_L \\ b'_L \end{pmatrix}_{Y=\frac{1}{6}}$$

$$\left(u_R\right)_{Y=\frac{2}{3}} \quad \left(c_R\right)_{Y=\frac{2}{3}} \quad \left(t_R\right)_{Y=\frac{2}{3}}$$

$$\left(d'_R\right)_{Y=-\frac{1}{3}} \quad \left(s'_R\right)_{Y=-\frac{1}{3}} \quad \left(b'_R\right)_{Y=-\frac{1}{3}}$$

Gauge Bosons

$$\gamma, Z, W^{\pm}, g_1, ..., g_8$$

Table 2.1: Standard Model fields. The $SU(2)_L \times U(1)_Y$ group representation of the fermion fields is explicitly shown.

Quarks carry a quantum number called *colour* which can take three different values. Coloured particles interact strongly through the exchange of gluons. Contrary to the elec-

trically neutral photon, gluons carry colour charge and hence couple to each other. This makes the strong force between two coloured particles increase with increasing distance.

Both quark and leptons carry *weak isospin* ($\vec{T}$) and *weak hyper-charge* (Y). These are quantum numbers that define the transformation under the $SU(2)_L \times U(1)_Y$ group. The $W^{\pm}$ and Z bosons couple to these "weak charges". As shown in Table 2.1, the left-(right-)handed fields transform as weak isospin doublets(singlets). As a consequence, Ws couple only to the left-handed fermions (with the spin oriented opposite to the direction of motion).

The $[d', s', b']$ weak isospin eigenstates are lineal combinations of the $[d, s, b]$ mass eigenstates. The unitary matrix relating both is the Cabbibo-Kobayashi-Maskawa matrix, which depends on four fundamental parameters of the SM: three angles and a phase. The latter provides the only mechanism within the SM that can account for the obserbed violation of CP symmetry.

The spin-1 field mediating the interactions results from the local gauge invariance of the SM Lagrangian. However, such a high degree of symmetry makes initially the theory unphysical since it predicts massless gauge bosons, while we know that for a realistic theory we need massive weak vector bosons. This problem is solved if we consider that the $SU(2)_L \times U(1)_Y$ symmetry is *spontaneously broken*.

The spontaneous symmetry breaking (SSB) mechanism is a general phenomenon which happens when the symmetric solutions of a theory are unstable and the ground state of the system is degenerated. Even if the theory is spontaneously broken, the symmetry is (in a sense) still present; it is only "hidden" by the choice of ground state. In spite of the SSB the theory can be shown to remain renormalizable [3]. This is an important property, as the renormalizability ensures that once a few parameters are determined experimentally, quantitative predictions can be calculated to arbitrary accuracy as a perturbative expansion in the coupling constant.

Therefore, in the SM the masses of the gauge fields (as well as of the fermions) are generated by SSB, ensuring that one of them (the photon) remains massless. The latter is attained by choosing a vacuum (the ground state in a quantum field theory) which only possesses $U(1)_{EM}$ symmetry. As a result of the SSB mechanism, the existence of a physical scalar particle is predicted in the minimal version of the SM, the so called Higgs boson [4].

The Higgs boson has not been observed experimentally yet, but some "hints" consistent with the production of the Higgs boson with a mass near 114 GeV/c^2 were found during the year 2000 [5]. The electroweak precision measurements made at LEP1, SLD and ν-Nucleon scattering experiments have some sensitivity to $\log(M_H)$ through loop corrections, and allow to constrain $\log(M_H)$ to be $1.78^{+0.27}_{-0.28}$ at 68% confidence level [6].

2.3 The Perturbative Theory of Strong Interactions

The most fundamental statement of QCD is that hadronic matter is made of quarks. This idea was born from the need to have a physical manifestation for the $SU(3)$ symmetry of flavour observed in the spectrum of the lowest-mass mesons (two-quark states) and baryons (three-quark states). The quarks in the baryons have to be half-integral spin states in order to account for the spins of low-mass baryons. In particular the quarks in a spin-3/2 baryon are in a symmetrical state of space, spin and $SU(3)_f$ degrees of freedom. Then the introduction of the colour degree of freedom was needed to avoid a violation of the Fermi-Dirac statistics.

A colour quantum number (QN) a is then carried by each quark. This QN can take three values (namely, red, green and blue) and in this QN the baryon wave functions are totally antisymmetric. In order not to create a proliferation of states with the introduction of this QN, the requirement is added that only colour singlet states can exist in nature. This lead to $SU(3)$ to be the group of colour transformations, with the quarks transforming according to the fundamental representation and antiquarks according to the complex conjugate one. The experiments thought to prove the existence of such point-like constituents went further than expected. The quarks were found to be not enough to explain the properties of hadrons. It was in this context that the QCD improved parton model [7] was constructed, with coloured quarks and gluons as the (up to now) final constituents of matter. The last fundamental statement came to explain why free quarks are not observed in nature. If they are not observed then a strong interaction should bind them together to form hadrons. *Asymptotic freedom* predicts that the coupling of quarks and gluons is large at large distances so as to confine quarks. At the same time the coupling is predicted to be small at short distances so that the quarks behave as free particles at asymptotically large energies.

2.3.1 The Lagrangian of Strong Interactions

The QCD Lagrangian density is given by

$$\mathcal{L}_{QCD} = \sum_{flavours} \bar{q}_a (i\gamma^\mu D_\mu - m_q)_{ab} q_b - \frac{1}{4} F^A_{\mu\nu} F^{A\mu\nu} + \mathcal{L}_{gauge-fixing} + \mathcal{L}_{ghost} \tag{2.1}$$

where the sum runs over the N_f different flavours of the quarks. The first two terms describe the interaction of spin-1/2 quarks of mass m and massless spin-1 gluons. $F^A_{\mu\nu}$ is the field strength tensor derived from the gluon field $\mathcal{A}^A_\alpha$ as

$$F^A_{\alpha\beta} = [\partial_\alpha \mathcal{A}^A_\beta - \partial_\beta \mathcal{A}^A_\alpha - g f^{ABC} \mathcal{A}^B_\alpha \mathcal{A}^C_\beta] \tag{2.2}$$

where the capital indices run over the eight colour degrees of freedom of the gluon field, g is the coupling constant which determines the strength of the interaction between coloured quanta, and f^{ABC} are the structure constants of the colour group, $SU(3)$. The third term in Eq. 2.2 shows the non-Abelian nature of QCD, which distinguishes this theory from QED. It gives rise to triplet and quartic gluon self-interactions and, ultimately, to asymptotic freedom. In non-Abelian theories, the covariant gauge-fixing term must be supplemented by a *ghost* term, which will not be discussed here as it is not relevant for what follows.

The quark fields q_a in Eq. 2.1 are in the triplet representation of the colour group and D is the covariant derivative, which acting on triplet fields takes the form:

$$(D_\alpha)_{ab} = \partial_\alpha \delta_{ab} + ig \left(t^C \mathcal{A}^C_\alpha\right)_{ab} \tag{2.3}$$

where the generators of $SU(3)$, t, are matrices in its fundamental representation and fulfill the relation

$$\left[t^A, t^B\right] = i f^{ABC} t^C \quad . \tag{2.4}$$

By convention the normalization of the $SU(N)$ matrices is chosen to be

$$T_r \left(t^A t^B\right) = T_R \delta^{AB}, \qquad T_R = \frac{1}{2} \quad . \tag{2.5}$$

With this choice, the colour matrices obey the following relations:

$$\sum_A t^A_{ab} t^A_{bc} = C_F \delta_{ac}, \qquad C_F = \frac{N^2 - 1}{2N} \tag{2.6}$$

$$\sum_{A,B} f^{ABC} f^{ABD} = C_A \delta^{CD}, \qquad C_A = N. \tag{2.7}$$

Thus for the specific case of $SU(3)$ we have

$$C_F = \frac{4}{3}, \qquad C_A = 3 \tag{2.8}$$

which are called the *colour factors*. They are related to the emission of a gluon by a quark and the splitting of a gluon into two other gluons, respectively. On the other hand, T_R in Eq. 2.5 is related to the rate of gluon splitting into quarks of one flavour.

2.3.2 Gauge Invariance

The QCD Lagrangian is invariant under local gauge transformations, i.e. the quark fields can be redefined independently, but not arbitrarily, at every point in space-time without changing the physical content. The behaviour of a quark field under such a local transformation is:

$$q_a(x) \to \exp\left(it \cdot \theta(x)\right) q_b(x) \tag{2.9}$$

and the covariant derivative is so called because it transforms in the same way as the field itself:

$$D_\alpha q(x) \to \exp\left(it \cdot \theta(x)\right) D_\alpha q(x) \quad . \tag{2.10}$$

From the previous equations the transformation of the gluon gauge field and the field strength can be obtained (see e.g. reference [8]) and it is observed that, in contrast to QED, the QCD field strength is not gauge invariant due to the self-interaction of gluons.

There is no gauge-invariant way of including a gluon mass, because the term $m^2 \mathcal{A}^\alpha \mathcal{A}_\alpha$ is not gauge invariant. This property is similar to QED where a massive photon is forbidden.

The gauge fixing explicitly breaks gauge invariance. However, in the end physical results will be independent of the gauge. The *ghost* term, that supplements the covariant gauge-fixing term, cancels the unphysical degrees of freedom of the gluon.

2.3.3 The Running Coupling

In a quantum field theory the calculation of a dimensionless observable R as a perturbation series in $\alpha_s = g/4\pi$, where R depends on a large energy scale Q, requires renormalization

to remove ultraviolet divergences. Such divergences come from loop corrections, such as those depicted in Fig. 2.2, which diverge for infinitely large momenta.

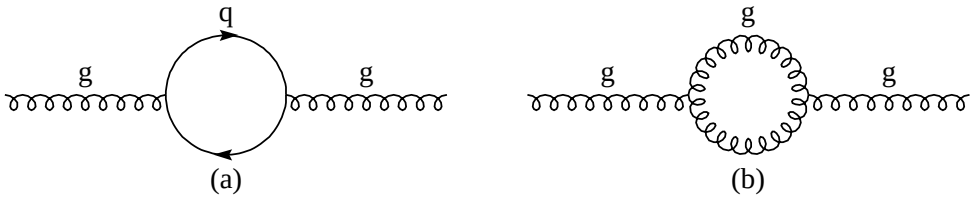

Figure 2.2: Loop corrections to the gluon propagator: (a) quark loop , (b) gluon loop.

Through renormalization the divergent terms are absorbed into the "bare" quantities of the theory, such as the coupling, the masses or the field normalizations, which are not observables, thus defining new renormalized quantities, which are measurable. This process introduces a second mass scale μ, at which the subtractions which remove the divergences are performed. R depends on the non-constant ratio Q/μ. The renormalized coupling also depends on μ.

Since μ is an arbitrary parameter, R cannot depend on μ when the coupling is fixed. Moreover, since R is dimensionless, it can only depend on Q^2/μ^2 and on the renormalized coupling α_s. Hence

$$\mu^2 \frac{d}{d\mu^2} R\left(\frac{Q^2}{\mu^2}, \alpha_s\right) \equiv \left[\mu^2 \frac{\partial}{\partial \mu^2} + \mu^2 \frac{\partial \alpha_s}{\partial \mu^2} \frac{\partial}{\partial \alpha_s}\right] R = 0 \tag{2.11}$$

which is called the renormalization group equation. Introducing $\tau = \ln\left(\frac{Q^2}{\mu^2}\right)$, and $\beta(\alpha_s) \equiv \mu^2 \frac{\partial \alpha_s}{\partial \mu^2}$, the renormalization group equation can be written as

$$\left[-\frac{\partial}{\partial \tau} + \beta(\alpha_s) \frac{\partial}{\partial \alpha_s}\right] R = 0 \tag{2.12}$$

which is solved by defining the running coupling $\alpha_s(Q)$,

$$\tau = \int_{\alpha_s}^{\alpha_s(Q)} \frac{dx}{\beta(x)} \tag{2.13}$$

where $\alpha_s(\mu) \equiv \alpha_s$. Thus all scale dependence in R comes from the running of $\alpha_s(Q)$. A change in the renormalization scale is compensated by a change of the coupling, and the physical observable R remains independent of the unphysical scale μ^2. However, this only holds if R is calculated at all orders of α_s, otherwise an explicit scale dependence appears at one order higher than the order at which the variable has been calculated.

The Beta Function

The running of the QCD coupling, α_s, is determined by the QCD β function, which has the expansion:

$$\beta(\alpha_s) = -b\alpha_s^2 \left(1 + b'\alpha_s + \mathcal{O}(\alpha_s^2)\right) \tag{2.14}$$

where

$$b = \frac{11C_A - 2N_f}{12\pi} \qquad b' = \frac{17C_A^2 - 5C_A N_f - 3C_F N_f}{2\pi(11C_A - 2N_f)} \tag{2.15}$$

with N_f the number of active flavours.

The β coefficients in general depend on the renomalization scheme used, hence also the running coupling. In this analysis the modified minimal subtraction renormalization scheme ($\overline{\mathrm{MS}}$) is used. The first two terms of the expansion for β are, in fact, scheme independent. From the definition of the β function and neglecting b' and higher order coefficients in Eq. 2.14 the following solution can be extracted,

$$\alpha_s(Q^2) = \frac{\alpha_s(\mu^2)}{1 + \alpha_s(\mu^2) b \ln \frac{Q^2}{\mu^2}} \quad . \tag{2.16}$$

Quark loop diagrams contribute to the negative N_f term in b, while gluon loop diagrams give a positive C_A contribution which makes an overall negative β function. This is in contrast to QED, where the b coefficients have opposite signs. Then, as Q becomes large, $\alpha_s(Q)$ decreases to zero. This property of QCD, which depends on the sign of b, is called asymptotic freedom. It is this property that allows reliable predictions from perturbation theory for processes involving high momentum transfers. In QED where b is negative, the coupling increases at large Q.

2.3.4 The Lambda Parameter

Perturbative QCD tells us how $\alpha_s(Q)$ varies with Q, but its absolute value has to be obtained from experiment. Nowadays, the value of the coupling at $Q = \mathrm{M_Z}$ is used as the fundamental parameter , which is a convenient reference scale large enough to be in the perturbative regime.

However, it is also useful to express $\alpha_s(Q)$ in terms of a dimensionfull parameter (constant of integration) Λ,

$$\ln \frac{Q^2}{\Lambda^2} = -\int_{\alpha_s(Q)}^{\infty} \frac{dx}{\beta(x)} = \int_{\alpha_s(Q)}^{\infty} \frac{dx}{bx^2(1+b'x+...)} \quad . \tag{2.17}$$

Then, if the perturbative theory were the whole story, $\alpha_s(Q) \to \infty$ as $Q \to \Lambda$. Thus Λ sets the scale at which $\alpha_s(Q)$ becomes large.

In next-to-leading order (NLO) we have

$$\alpha_s(Q) = \frac{1}{b\ln(Q^2/\Lambda^2)}\left[1 - \frac{b'}{b}\frac{\ln\ln(Q^2/\Lambda^2)}{\ln(Q^2/\Lambda^2)}\right] \quad . \tag{2.18}$$

The Λ parameter depends on the number of active flavours, N_f, where active means $m_q \lesssim Q$. Thus for $5 \lesssim Q \lesssim 175$ GeV, $N_f = 5$. It also depends on the renormalization scheme. So, taking as current best fit value of α_s at the Z pole [9]

$$\alpha_s(\mathrm{M_Z}) = 0.1184 \pm 0.0031 \tag{2.19}$$

the corresponding preferred value of $\Lambda_{\overline{\mathrm{MS}}}$ for $N_f = 5$ falls in the range:

$$178 \text{ MeV} < \Lambda_{\overline{\mathrm{MS}}}(5) < 251 \text{ MeV}.$$

2.4 The Non-Perturbative Regime of Strong Interactions

The transition from the quark and gluon degrees of freedom appropriate in perturbation theory to the hadrons observed by real world experiments is poorly understood. In this strongly interacting transition regime we presently rely on models, which to varying degrees reflect possible scenarios for the QCD dynamics.

Corresponding to asymptotic freedom at high momentum scales (short distances), we have infrared slavery: $\alpha_s(Q)$ becomes large at low momenta (long distances). pQCD is not reliable anymore, and non-perturbative methods, such as lattice calculations, must be used. Lattice QCD is QCD formulated on a discrete Euclidean space-time grid. The discrete space-time lattice acts as a non-peturbative regularization scheme. At finite values of the lattice spacing a there are no infinities. Furthermore, renormalized physical quantities have a finite well behaved limit as $a \to 0$. This subfield of the particle theory attempts to solve QCD problems in the regime of the nuclear matter, i.e. at the scale of the hadronic world. Its aim is the calculation of correlation functions of hadronic operators and matrix elements of any operator between hadronic states in terms of the

fundamental quark and gluon degrees of freedom.

There are two important low momentum-scale phenomena:
Confinement: partons (quarks and gluons) are found only in colour-singlet bound states, called hadrons, of size ≈ 1 fm. If an attempt to isolate the partons within a hadron is done, it becomes energetically favourable to create extra partons, forming additional hadrons. This is a static (long-distance) property of QCD, which can be treated by lattice techniques.
Hadronization: partons produced in short distance interactions reorganize themselves (and multiply) to make the observed hadrons. This is a dynamical (long-timescale) phenomenon, where only phenomenological models are available at present.

2.4.1 Infrared Divergences

Even in the high-energy, short-distance regime, long-distance aspects of QCD cannot be ignored. Soft or collinear gluon emission gives infrared divergences in pQCD. Light quarks ($m_q \ll \Lambda$) also lead to divergences in the limit $m_q \to 0$.

pQCD can still be used to perform calculations, provided that the study is limited to two classes of observables:

Infrared- and collinear-save quantities, i.e. those insensitive to soft or collinear branching. Infrared divergences in pQCD either cancel between real and virtual contributions or are removed by restricting the phase space through an integration cut-off. Such quantities are determined primarily by hard, short-distance physics; long-distance effects give power corrections, suppressed by inverse powers of a large momentum scale.

Factorizable quantities, i.e. those in which infrared sensitivity can be absorbed into an overall non-perturbative factor, to be determined experimentally.

2.5 The implementation of QCD in Monte Carlo Models

The whole chain, from the e^+e^- annihilation to the hadronization and decay of unstable hadrons, has been implemented in Monte Carlo programs, which make it possible to generate multihadronic final states. An important aspect of the hadronic decay of the Z boson is that the final state hadrons generally form jets, i.e. they are not arbitrarily spread out in phase space, but stay rather close together (see Fig. 2.3). The direction and energies of these jets are in close correspondence with the directions and energies of the primary high energetic partons. More precisely, hadrons are formed out of the colour

field with limited transverse momentum, which is independent of the hard energy scale. Therefore, the higher the energy of the primary parton, the stronger is the collimation of hadrons around its direction. An event, where the primary quarks do not radiate any energetic gluons will typically appear as two back-to-back "bundles" of hadrons, whereas events with one or more high energy gluons, radiated off at sufficiently large angles, will give rise to additional hadronic jets.

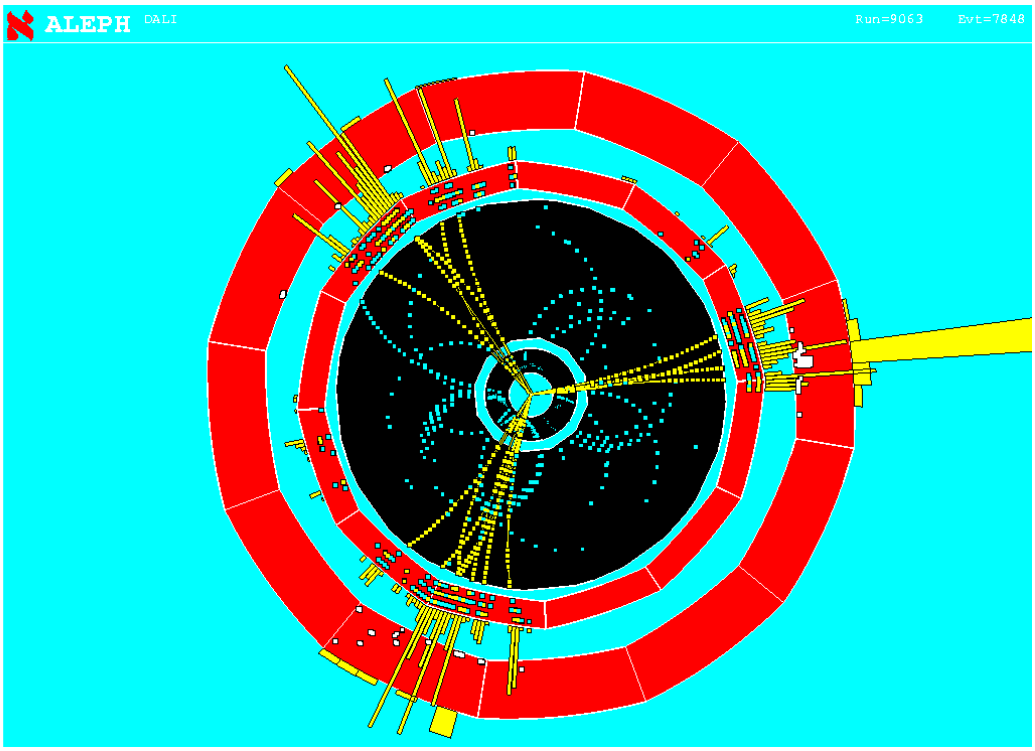

Figure 2.3: A three-jet hadronic event recorded with the ALEPH detector.

The most popular Monte Carlo programs that try to simulate all the properties of the electron-positron annihilation into hadrons are PYTHIA (JETSET) and HERWIG [10, 11]. PYTHIA combines a *Parton Shower* (PS) algorithm with the Lund string fragmentation. HERWIG is also based on a PS, but models the hadronization via cluster fragmentation. Some details about the PS implementation and about the string and cluster fragmentation models are given in the following sections.

2.5.1 Perturbative QCD: the approximation through a Parton Shower

Complete perturbative calculations in QCD have been performed only to next-to-leading order in most cases, or to one further order in α_s for a few observables. The effort for the calculation of a new term increases roughly factorially with the order, so not many more higher-order terms are expected to be calculated soon. Nevertheless there are regions of phase space in which higher-order terms are enhanced and cannot be neglected.

In the present section an approximate result in which such enhanced terms are taken into account to all orders will be shown. This will lead to a physically appealing parton shower picture which can readily be implemented in computer simulations. The parton shower represents an approximate perturbative treatment of QCD dynamics at scales of momentum transfer-squared t greater than some infrared cut-off value t_0, typically taken to be of the order of 1 GeV^2.

Parton Branching

Assume the branching of a parton a into $b + c$ as shown in Fig. 2.4. a is defined as an outgoing parton, i.e. the time-like branching is chosen. The opening angle is $\theta = \theta_b + \theta_c$ and the energy fraction is $z = E_b/E_a = 1 - E_c/E_a$. Thus, for small angles and massless partons, where the matrix element is enhanced, the following expression holds,

$$t = 2E_bE_c\,(1 - \cos\theta) = z(1 - z)E_a^2\theta^2 \tag{2.20}$$

hence, using transverse momentum conservation,

$$\theta = \frac{1}{E_a}\sqrt{\frac{t}{z(1 - z)}} = \frac{\theta_b}{1 - z} = \frac{\theta_c}{z} \quad . \tag{2.21}$$

Consider the different cases, i.e. a,b and c being gluons, a being a gluon and b and c a quark-antiquark pair, and a and b being quarks and c a gluon. Then the unregularized Dokshitzer-Gribov-Lipatov-Altarelli-Parisi (DGLAP) splitting kernels can be obtained (a detailed calculation can be found in [8]):

$$\hat{P}_{qq}(z) = C_F\frac{1 + z^2}{1 - z} \tag{2.22}$$

$$\hat{P}_{gg}(z) = C_A\frac{(1 - z(1 - z))^2}{z(1 - z)} \tag{2.23}$$

$$\hat{P}_{qg}(z) = T_F\left(z^2 + (1 - z)^2\right) \tag{2.24}$$

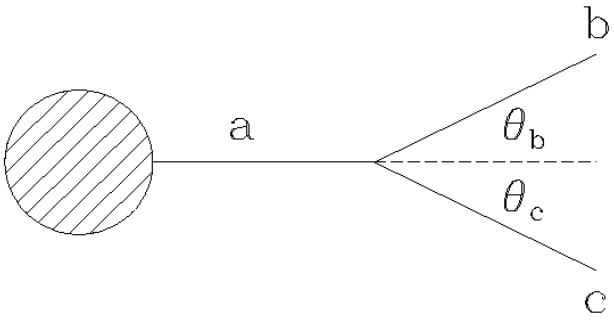

Figure 2.4: Kinematics of time-like parton branching.

The cross section for the various branching processes can be written as:

$$d\sigma_{n+1} = d\sigma_n \frac{dt}{t} dz \frac{\alpha_s}{2\pi} \hat{P}_{ba}(z) \quad . \tag{2.25}$$

A simple probabilistic picture can be adopted here. The cross section in n-th order is corrected by the probability for the additional branching of an outgoing parton, and this probability is given by $\alpha_s \, \hat{P}(z) dz \, dt/t$. The integration over a properly defined phase-space region will then lead to

$$\sigma_n \propto \alpha_s^n L^m, \quad m = 2n, 2n-1, ... \tag{2.26}$$

with L again some logarithm of a cut-off parameter in order to avoid singular regions. When approaching singular regions of the phase space, this logarithm will grow, and even for small α_s one will find large corrections. It becomes clear that the effective perturbative expansion parameter is not α_s any more, but rather $\alpha_s L$ or $\alpha_s L^2$, which can approach $\mathcal{O}(1)$ for a large logarithm. Hence the series in this new expansion parameter has to be resummed in all orders, if a meaningful prediction from perturbative theory ought to be obtained. This can be done through the solution of evolution equations, which are introduced in the next section.

The DGLAP Evolution Equations

The DGLAP evolution equations are typically derived within the framework of deep-inelastic scattering (see for example [8]). These are space-like processes, however, similar evolution equations can also be derived for time-like processes such as e^+e^- annihilation into $q\bar{q}$ with subsequent gluon radiation. For simplicity, we consider only a single type of

branching, the multiple gluon emission from a time-like quark, originating from a Z decay. A quark with initial virtuality $\approx Q^2$ evolves down in virtuality via successive small-angle gluon emissions. Eventually a lower scale t_0 is reached where non-perturbative (long-distance) effects become dominant.

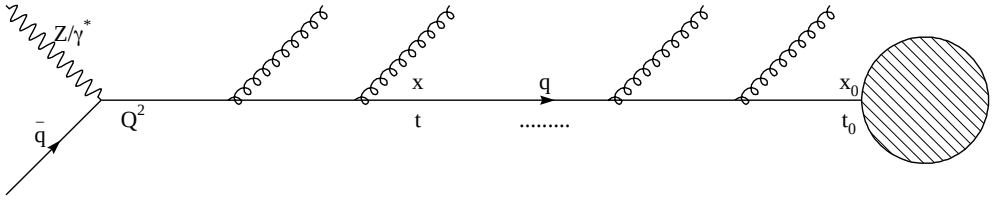

Figure 2.5: Final state branching in $e^+e^- \to q\bar{q}$.

The momentum fraction distribution, fraction with respect to the initial momentum, $D(x,t)$ of the evolving quark at some scale t gets infinitely large contributions from arbitrarily soft and collinear gluon radiation if the scale is small. However, the change of the distribution at some scale caused by additional radiation of a gluon is calculable. First we introduce a pictorial representation of the evolution, where every sequence of branchings is represented by a path in (t,x)-space, see Fig. 2.6. Each branching corresponds to a step downwards, from a higher to a lower value of the momentum fraction x, at a value of t equal to the virtual mass-squared after the branching. The change in the parton distribution $D(x,t)$ when t is increased to $t+\delta t$ is just the number of paths arriving in the element $(\delta t, \delta x)$ minus the number leaving that element, divided by δx. To find the total number arriving, we must integrate the branching probability times the parton density over all higher momentum fractions $x' = x/z$, to obtain

$$\begin{aligned} \delta D(x,t) &= \frac{\delta t}{t}\int_x^1 dx' dz \frac{\alpha_s}{2\pi}\hat{P}(z) D(x',t)\delta(x-zx') \\ &= \frac{\delta t}{t}\int_0^1 \frac{dz}{z}\frac{\alpha_s}{2\pi}\hat{P}(z) D(x/z,t) \end{aligned} \tag{2.27}$$

where $\hat{P}(z)$ is the relevant unregularized splitting function. For the number leaving the element, we integrate instead over all lower momentum fractions $x' = zx$:

$$\begin{aligned} \delta D_{out}(x,t) &= \frac{\delta t}{t} D(x,t)\int_0^x dx' dz \frac{\alpha_s}{2\pi}\hat{P}(z)\delta(x'-zx) \\ &= \frac{\delta t}{t} D(x,t)\int_0^1 dz \frac{\alpha_s}{2\pi}\hat{P}(z) \end{aligned} \tag{2.28}$$

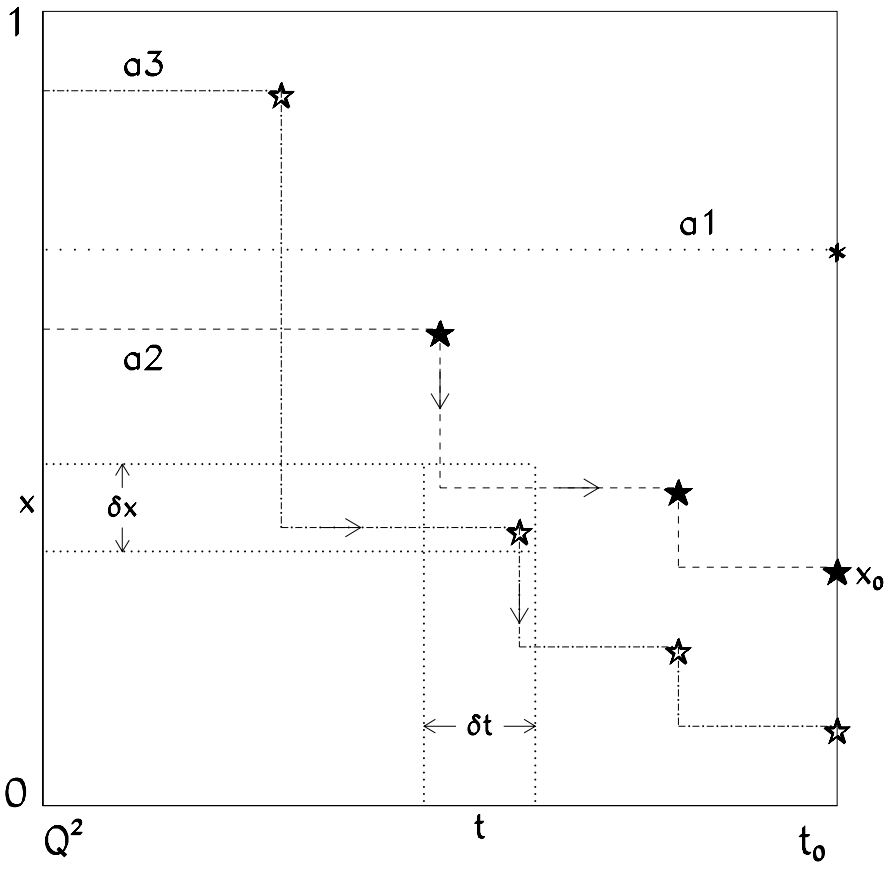

Figure 2.6: Representation of parton branching by paths in (t,x)-space. Three possible paths are indicated.

The net change in the population of the element is thus

$$\delta D(x,t) = \delta D_{in} - \delta D_{out} = \frac{\delta t}{t}\int_0^1 dz \frac{\alpha_s}{2\pi}\hat{P}(z)\left[\frac{1}{z}D(x/z,t) - D(x,t)\right]. \tag{2.29}$$

The singularity at $z = 1$ in $\hat{P}(z)$ is damped by the difference $[\frac{1}{z}D(\frac{x}{z},t) - D(x,t)]$, thus the whole expression is well defined. A compact notation is obtained by the introduction of the *plus-prescription*

$$\int_0^1 dx f(x)g(x)_+ = \int_0^1 dx\,[f(x) - f(1)]\,g(x). \tag{2.30}$$

Using this plus-prescription, the regularized splitting functions are defined

$$P(z) = \hat{P}(z)_+ \tag{2.31}$$

in terms of which the evolution equation for the parton density may be written as

$$t\frac{\partial}{\partial t}D(x,t) = \int_x^1 \frac{dz}{z}\frac{\alpha_s}{2\pi}P(z)D(x/z,t). \tag{2.32}$$

When there are several different types of partons in the branching process, the evolution equation has to be generalized to take into account the different processes by which a parton of type i can enter or leave the element $(\delta t, \delta x)$. This leads to a coupled set of evolutions equations of the form

$$t\frac{\partial}{\partial t}D_i(x,t) = \sum_j \int_x^1 \frac{dz}{z}\frac{\alpha_s}{2\pi}P_{ij}D_j(x/z,t)\,. \tag{2.33}$$

The above formulation of the DGLAP equations is convenient for obtaining analytical solutions for the evolution of parton distributions. Introducing the *Sudakov form factor*

$$\Delta(t) \equiv \exp\left[-\int_{t_0}^t \frac{dt'}{t'}\int dz\frac{\alpha_s}{2\pi}\hat{P}(z)\right]\,, \tag{2.34}$$

we can write Eq. 2.32 as

$$t\frac{\partial}{\partial t}D(x,t) = \int \frac{dz}{z}\frac{\alpha_s}{2\pi}\hat{P}(z)D(x/z,t) + \frac{D(x,t)}{\Delta(t)}t\frac{\partial}{\partial t}\Delta(t) \tag{2.35}$$

and hence

$$t\frac{\partial}{\partial t}\left(\frac{D(x,t)}{\Delta(t)}\right) = \frac{1}{\Delta(t)}\int \frac{dz}{z}\frac{\alpha_s}{2\pi}\hat{P}(z)D(x/z,t)\,. \tag{2.36}$$

This equation can be integrated to give an integral equation for $D(x,t)$ in terms of the initial parton distribution $D(x,t_0)$:

$$D(x,t) = \Delta(t)D(x,t_0) + \int_{t_0}^t \frac{dt'}{t'}\frac{\Delta(t)}{\Delta(t')}\int \frac{dz}{z}\frac{\alpha_s}{2\pi}\hat{P}(z)D(x/z,t')\,. \tag{2.37}$$

The first term on the right-hand side is the contribution from paths that do not branch between scales t and t_0. Thus the Sudakov form factor $\Delta(t)$ is simply the probability of evolving from t to t_0 without branching. The second term is the contribution from all paths which have their last branching at scale t'. The factor $\Delta(t)/\Delta(t')$ represents the probability of evolving from t to t' without branching.

In the present discussion for the Sudakov form factor, the infrared singularity of the unregularized splitting functions at $z = 1$ has been ignored. However, this singularity is removed, in order for the form factors to be defined, through an infrared cut-off, $z < 1 - \epsilon(t)$. Branchings with z above this range are classified as *unresolvable*: they involve emission of an undetectable soft parton. The Sudakov form factor with this cut-off

then gives the probability of evolving from t to t_0 without any resolvable branching.

Although no virtual corrections have been mentioned explicitly, the Sudakov form factor in fact sums enhanced virtual (parton loop) as well as real (parton emission) contributions to all orders. The virtual corrections affect the no-branching probability, and are included via unitarity, which is just the fact that the sum of the branching and no-branching probabilities must be unity. The resolvable branching probability tells us via unitarity the sum of the virtual and unresolvable real contributions: the latter two are both divergent but their sum is finite, and included consistently in Eq. 2.36.

A natural cut-off for the branching would be that the virtual mass-squared $t > t_0$, which can be translated into

$$z(1-z) > t_0/t \quad . \tag{2.38}$$

This follows from the condition of positive transverse momentum, as shown in [8],

$$p_\perp^2 = z(1-z)p_a^2 - (1-z)p_b^2 - zp_c^2 > 0 \tag{2.39}$$

and $p_a^2 = t, p_b^2, p_c^2 > t_0$. The cut-off condition can be approximated to

$$\frac{t_0}{t} < z < 1 - \frac{t_0}{t}\,. \tag{2.40}$$

A further refinement consists in the usage of the running coupling with a properly chosen scale. As a first guess, the scale for the running could be set to the virtuality of the branching parton. However, a more careful treatment suggests [12] that $z(1-z)t$ should be used as its argument, which is essentially the transverse momentum squared. By doing this , terms of the form $\ln(1-z)/(1-z)$ are resummed, which are found in next-to-leading calculations of the splitting functions.

Finally the Sudakov form factor for a single branching type becomes

$$\Delta(t) = \exp\left[-\int_{2t_0}^{t}\frac{dt'}{t'}\int_{t_0/t'}^{1-t_o/t'} dz\frac{\alpha_s[z(1-z)t']}{2\pi}\hat{P}(z)\right]\,. \tag{2.41}$$

Monte Carlo Method

The formulation of parton branching in terms of the Sudakov form factor is well suited to computer implementation, and is the basis of the parton shower Monte Carlo programs for simulating QCD jets. The basic Monte Carlo branching algorithm in its simplest form

is described in the following lines, neglecting the complications for the different possible branchings and QCD coherence effects.

The basic problem that the Monte Carlo branching algorithm has to solve is as follows: given the virtual mass scale and momentum fraction (t_1, x_1) after some step of the evolution, or as initial conditions, generate the values (t_2, x_2) after the next step. The first quantity to be generated by the algorithm is the value of t_2. It was shown that for a time-like branching the probability of evolving from t_1 to t_2 without (resolvable) branching is $\Delta(t_1)/\Delta(t_2)$ where $\Delta(t)$ is the Sudakov form factor. Thus t_2 can be generated with the correct probability distribution by solving the equation

$$\frac{\Delta(t_1)}{\Delta(t_2)} = \mathcal{R} \tag{2.42}$$

where $\mathcal{R}$ is a random number distributed uniformly in the interval $[0, 1]$. If the value of t_2 is lower than t_0, this means that no further branching occurs. Otherwise, we have to generate the value of the momentum fraction $x = x_2/x_1$ for the next branching, with a probability distribution proportional to $(\alpha_s/2\pi)P(z)$, where $P(z)$ is the appropriate splitting function. This can be done by solving the equation

$$\int_{\epsilon}^{x_2/x_1} dz \frac{\alpha_s}{2\pi} P(z) = \mathcal{R}' \int_{\epsilon}^{1-\epsilon} dz \frac{\alpha_s}{2\pi} P(z) \tag{2.43}$$

where $\mathcal{R}'$ represents another random number in the interval $[0, 1]$ and ϵ is the infrared cut-off for resolvable branching.

The values of (t_i, x_i) generated by successive applications of the algorithm define the virtual masses and momentum fractions of the exchanged parton, from which the momenta of the emitted gluons can be computed. The azimuthal angles of their emission need to be specified by a further Monte Carlo algorithm. Each emitted gluon and in general each parton with time-like momentum in a parton shower, can itself undergo further branching, which can be dealt with by a similar algorithm. As a consequence of successive time-like branchings, a parton cascade develops. Each outgoing line becomes the source of a new cascade, until the Monte Carlo algorithm generates a no-branching step in the evolution of its virtual mass. Those that do branch produce partons of lower virtual masses, which become more likely to generate no branching. Eventually all outgoing lines have stopped branching and the cascade ceases. At this stage, which depends on the cut-off scale t_0, the outgoing partons have to be converted into hadrons via the hadronization model if the Monte Carlo program is to be used for the simulation of real events. Different available models are described in Section 2.5.2.

2.5.2 Soft QCD

The bulk properties of hadronic events in Z decay are established early in the fragmentation when virtualities are large and pQCD is valid. However, the issue of to what extent pQCD dominates and what are the contributions coming from non-perturbative effects is still under investigation.

It was already stated that the final state hadrons form jets with directions and energies quite close to the ones of the primary high energetic partons. The fact that soft QCD does not heavily modify the properties of these jets might be a result of several effects. First multiple gluon radiation is restricted in phase space such that subsequent soft gluons can not be radiated at arbitrarily large angles (this is called *angular ordering*). Second, the hadronization phase involves only small momentum transfers, thus the main topological properties of the event remain almost untouched.

Therefore, the interface between perturbative an soft QCD is implemented at two levels in Monte Carlo programs as HERWIG and PYTHIA, which are the ones used in the analyses described in Chapter 6. Soft Gluon Emission is introduced in the parton shower, which also includes our knowledge on pQCD. Then, at the end of the shower the partons undergo hadronization. Different models are used in the MCs, namely string and cluster models. In some cases the parton shower is not used, and the partons coming from the matrix element expressions are directly hadronized (this option is only implemented in PYTHIA).

i) **Soft Gluon Emission**

The parton branching formalism discussed so far takes account of collinear enhancements to all orders in perturbative theory. However, there are also soft enhancements due to gluon emission. The singularities of the small-angle parton splitting functions for soft gluon emission have already appeared in the previous section. However, the enhancement due to soft gluon emission has more general contributions. Whenever an external line of a QCD Feynman graph with momentum p and mass m (not necessarily small) emits a gluon with momentum q and energy ω, a divergence as $\omega \to 0$ appears for any velocity and emission angle. Notice that there is no soft enhancement of radiation from an off-mass-shell internal line of a Feynman graph, since the associated denominator factor does not diverge when $\omega \to 0$.

The enhancement factor in the amplitude for each external line implies that the cross section enhancement has a factor which is the sum over all pairs of external lines $\{i, j\}$ [8]:

$$d\sigma_{n+1} = d\sigma_n \frac{d\omega}{\omega} \frac{d\Omega}{2\pi} \frac{\alpha_s}{2\pi} \sum_{i,j} C_{ij} W_{ij} \tag{2.44}$$

where $d\Omega$ is the element of solid angle for the emitted gluon, C_{ij} is a colour factor, and the radiation function W_{ij} is given by

$$W_{ij} = \frac{\omega^2 p_i \dot{p}_j}{p_i \dot{q} p_j \dot{q}} = \frac{1 - v_i v_j \cos\theta_{ij}}{(1 - v_i \cos\theta_{iq})(1 - v_j \cos\theta_{jq})} \tag{2.45}$$

with v_i the velocity of the i-th particle. The radiation function can be separated into two parts, containing the collinear singularities along lines i and j. For simplicity we consider massless particles ($v_{\mathrm{i,j}} = 0$). Then, $W_{ij} = W_{ij}^i + W_{ij}^j$ where

$$W_{ij}^i = \frac{1}{2}\left(W_{ij} + \frac{1}{1 - \cos\theta_{iq}} - \frac{1}{1 - \cos\theta_{jq}}\right) \quad . \tag{2.46}$$

This function has the property of angular ordering. After the azimuthal averaging, the contribution of W_{ij}^i is confined to a cone, centered on the direction of i, extending in angle as far as the direction of line j.

Angular ordering is the coherence effect common to all gauge theories. In QED it causes the Chudakov effect, i.e. the suppression of soft bremsstrahlung from e^+e^- pairs. In QCD the angular ordering provides the basis for the coherent parton branching formalism, which includes soft gluon enhancements to all orders. For two external lines forming a colour singlet, as in $e^+e^- \to q\bar{q}$, the angular ordering operates as in QED suppressing the radiation outside the cones extending from i to j and vice-versa. A more interesting case is that of three partons (i, j, k) forming a colour singlet, such as $e^+e^- \to q\bar{q}g$. There, each of the partons i, j and k radiates in proportion to its colour charge squared. When i and j are close in angle, their incoherent contributions are limited (after azimuthal averaging) to cones of half-angle θ_{ij}. At larger angles, out to the direction of k, they give coherent contributions in proportion to their combined colour charge squared. This contribution can be computed as if it came from an internal line of momentum $p_l = p_i + p_j$, but in reality it comes coherently from the two external lines.

The above treatment can be extended to higher orders leading to a coherent parton branching formalism that can be used to compute soft gluon enhancement to all orders. The rules for coherent branching involve a simple modification of those for the collinear branching process seen in Section 2.5.1. Such modifications are detailed in [8] and they

lead to the Sudakov form factor for the coherent branching process,

$$\tilde{\Delta}(t) = \exp\left[-\int_{4t_0}^{t}\frac{dt'}{t'}\int_{\sqrt{t_0/t'}}^{1-\sqrt{t_0/t'}}\frac{dz}{2\pi}\alpha_s\left(z^2(1-z)^2t'\right)\hat{P}(z)\right]. \qquad (2.47)$$

ii) **Hadronization**

One general approach to hadronization, based on the observation that perturbation theory seems to work well down to rather low scales, is the hypothesis of local parton-hadron duality. Here one only supposes that the flow of momentum and quantum numbers at the hadron level tends to the flow established at the parton level. Thus, for example, the flavour of the quark initiating a jet should be found in a hadron near the jet axis. The extent to which the hadron flow deviates from the parton flow reflects the irreducible smearing of order Λ due to hadron formation. However more explicit hadronization models are needed in order to compute detailed predictions. The two classes of models used in the analysis of this thesis are briefly described in the following paragraphs.

String Model

In an e^+e^- annihilation, neglecting the possibility of gluon bremsstrahlung, the produced quark and antiquark move out in opposite direction, losing energy to the colour field, which is supposed to collapse into a string-like configuration between them. Mesons and baryons are created by tunneling effects or equivalently by the breakup of the colour tube. This *Lund Model* [13] is inspired by the idea that because of the self-coupling of the gluons, an effective anti-screening of the bare colour charge occurs and the field between colour charges is restricted to a flux tube. Hence describing the gluon field as a flux tube with constant energy per unit length, leading to a linearly rising potential, at increasing distance between colour charges the attractive force stays constant instead of decreasing, as is the case for the electro-magnetic force. Eventually the energy in the colour field becomes so large that $q\bar{q}$ pairs are created from the vacuum, which afterwards combine to form colour-neutral states. An schematic view of the string model is shown in Fig. 2.7.

Cluster Model

An important property of the parton branching process is the preconfinement of colour [14]. Preconfinement implies that the pairs of colour-connected neighbouring partons discussed above have an asymptotic mass distribution that falls rapidly at high masses and is asymptotically Q^2-independent and universal. This suggests a class of cluster hadronization models, in which gluons at the end of the perturbative phase are split into quark and antiquark pairs. Then, colour-singlet clusters of partons form which afterwards decay

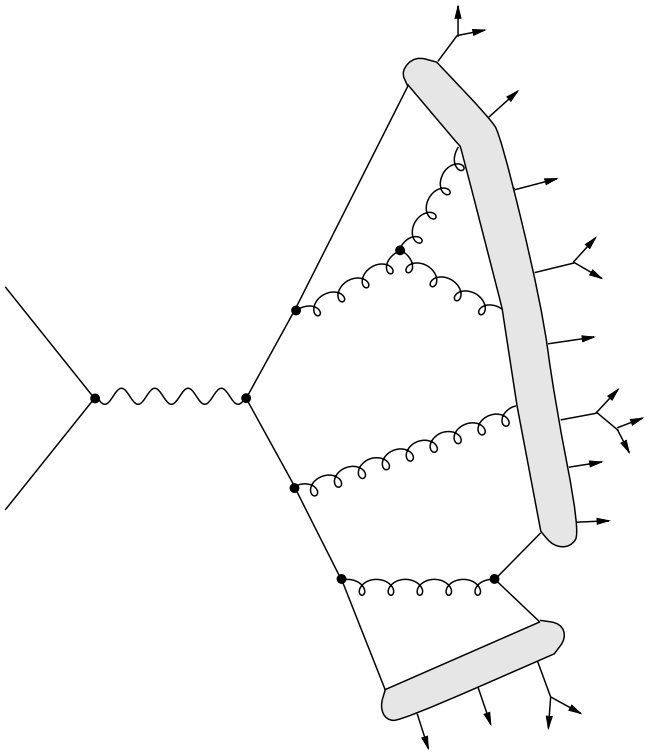

Figure 2.7: String fragmentation scheme.

isotropically into hadrons. Only these hadrons and/or the decay products of short-lived or weakly decaying ones are measurable in the detector. An schematic view of the cluster model is shown in Fig. 2.8.

2.5.3 Monte Carlo Programs: a brief description

Complete matrix elements (ME) calculations are expected to give a good description of multi-jet events when large separations among jets are involved and in particular when angular variables are considered. On the other hand, pure ME differential cross sections lack parton shower and hadronization and cannot reproduce collinear and soft radiation at arbitrarily high order. It is therefore important to have the possibility to start with pure ME calculations and complement them with these additional features. The results obtained in this way (ME + PS + hadronization) can be compared with pure parton level ones as well as those from dedicated QCD MCs, like standard $q\bar{q}$ PYTHIA and HERWIG.

If one takes for example topologies with four or more jets, one expects that a reasonable description for not too small values of the jet resolution y_{cut} may be obtained starting

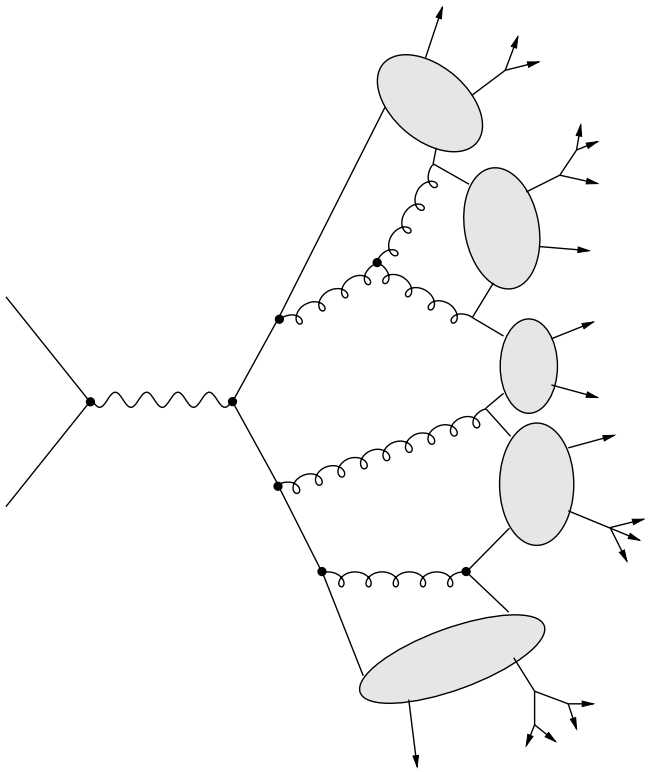

Figure 2.8: Cluster fragmentation scheme.

with a four-parton ME at a much lower y_{cut} and adding to it PS and hadronization. This jet resolution parameter, y_{cut}, introduced here is just a parameter of the different algorithms used to define jets at parton level in the theoretical calculations, and for grouping the selected neutral and charged tracks into jets at the experimental level. Even if events such as the one in Fig. 2.3 have been seen in a detector such as ALEPH, there is no unique way of grouping particles into jets and so different algorithms have been proposed. Basically, the method used is the successive binary clustering, i.e. for all pairs of final-state particles (i, j), a test variable y_{ij} is defined. The minimum of all y_{ij} is compared to the so-called jet resolution parameter. If it is smaller, the two particles are recombined into a new pseudo-particle with four-momentum $p_k = p_i + p_j$ (other recombination schemes have also been proposed).

One must however be aware of the fact that when starting with four-parton ME, all events described by two- or three-parton ME + PS + hadronization are not taken into account. In this respect QCD MCs surely give a more complete description as they start a PS from a two-parton ME and match three-parton production with the respective ME

results. The above mentioned approach of starting from four-parton ME can however be considered as a complementary approach for some studies and a way to check MC results when for instance angular variables or mass effects are involved.

In the following sections two options to start with four-parton configurations, using the PYTHIA showering and hadronization, are described. However, there are other options as the ones described in the HERWIG and APACIC subsections.

PYTHIA

A shower interface to four-partons massless matrix elements
Since version 6.1, the PYTHIA MC program contains an algorithm to start a shower from a given four-jet configuration, $q\bar{q}gg$ or $q\bar{q}q'\bar{q}'$. This allows comparisons of four-jet topologies between matrix-element calculations and data, with showering and hadronization effects better implemented, which are not covered by the matrix-element calculations alone.

The standard PYTHIA parton shower does not include any matching procedure to four-jet matrix elements. Therefore, it is not a good option for the description of four-jet topologies. For example, it does not correctly model angular azimuthal distributions in branchings. In fact, the standard shower routine is set up only to handle systems of two showering partons, not three or more.

The basic idea of matching to a four-parton configuration is to cast the output of matrix element generators in the form of a parton shower history, which then can be used as input for a complete parton shower. Here two of the subsequent branchings already have their kinematics defined, while the rest are chosen freely as in a normal shower. Benefits of having a prehistory include *(i)* the availability of the standard machinery to take into account recoils when masses are assigned to massless partons in the matrix elements, *(ii)* a knowledge of angular-ordering constraints on subsequent emissions and azimuthal anisotropies in them, and *(iii)* information on the colour flow as required for the subsequent string description. The choice among possible shower histories is based on a weight obtained from the mass poles and splitting kernels.

For example, let's concentrate on a process like $q\bar{q}gg$. Here the matrix-element expression contains contributions from five graphs (Fig. 2.9) and from interferences between them. The five graphs can also be read as five possible parton shower histories, but here

without the possibility of including interferences. The relative probability for each of these possible histories can be obtained from the rules of shower branchings.

The relative probability $\mathcal{P}$ for each of the five possible parton-shower histories can be used to select one of the possibilities at random. Then, when the conventional parton shower algorithm is executed, the properties such as masses, momentum transfers and angles between mother and daughter partons are forced to stay at the same value as for the ME configurations. However, this forcing cannot be exact since the final partons given by the ME are on the mass shell, while the corresponding partons in the parton shower might be virtual and branch further. All other branchings of the parton shower are selected at random according to the standard evolution scheme. Singular regions are typically avoided with a cut $y > y_{\rm int}$(default 0.01), where y is the square of the minimal scaled invariant mass between any pair of partons. All this is done by calling the PY4JET routine that will shower and fragment the four-parton configuration given as input. The partons have to be stored in the order $q\bar{q}gg$ or $q\bar{q}q'\bar{q}'$, where $q'\bar{q}'$ is assumed to be the secondary quark pair.

This strategy used in PYTHIA has the advantage that it can be applied to arbitrarily complicated partonic states, but the disadvantage that it does not tell how to mix different event topologies consistently. Therefore, it can be used for events where the main partons are well separated, and the task is to provide a realistic representation of the internal structure of the resulting jets, which is the case of a four-parton configuration at LEP1.

Interfacing four-parton massive matrix elements: FOURJPHACT
FOURJPHACT is a Fortran code that computes exact LO *massive* MEs for all $e^+e^- \to q\bar{q}q'\bar{q}'$ and $e^+e^- \to q\bar{q}gg$ final states and it interfaces them with the PYTHIA routine PY4JET.

The program starts by computing some cross section, where one can choose between fixed or running α_s. Unweighted events may be generated during this step, or in a second run in order to obtain a predetermined number of events. These may be passed to PYTHIA which provides PS and hadronization.

An inventory of cuts at parton level are already defined in FOURJPHACT: to implement them one only has to specify the numerical values for minima and maxima of

energies, transverse momenta, angles among partons and invariant masses. In a similar way, cuts using the resolution parameter of the most used clustering algorithms can be requested (e.g. a DURHAM y_{cut}, which is the clustering algorithm used for this thesis, as explained in Section 5.1).

FOURJPHACT can compute or generate events for one final state at a time or for all 20 final states with quarks (no top) and gluons at the same time. In this last case, the corresponding probability of each channel is determined or read from a file, and the generated events will have the correct fraction of all final states. This "one shot" option is often used when hadronization is required afterwards.

HERWIG

Four-jet matrix element + parton shower options (massless ME)
A new option available in HERWIG version 6.1 is to generate events starting from the four-parton processes $e^+e^- \to q\bar{q}gg$ and $e^+e^- \to q\bar{q}q'\bar{q}'$. The relevant process code is $IPROC = 600 + IQ$ for primary quark flavour IQ or 600 for a sum over all flavours. The matrix elements used are those of Ellis, Ross and Terrano [15] and Catani and Seymour [16], which include the relative orientation of initial and final states, but not quark masses. The kinematic effects of quark masses are taken into account in the subsequent parton showers and in matching the showers to the momentum configurations generated according to the matrix elements. The variable $EMSCA = \min \sqrt{s_{ij}}$, where $s_{ij} = 2p_i \cdot p_j$, sets a limit on the transverse momenta in the showers and is also used as the scale for α_s. The latter feature has the effect of enhancing the regions of small s_{ij} relative to matrix element calculations with α_s fixed.

To avoid soft and collinear divergences in the matrix elements, an internal parton resolution parameter $Y4JT$ must be set. The interparton distance is calculated using either the DURHAM or JADE metric. This choice is governed by the logical parameter $DURHAM$. For reliability of the results, one should use the same metric for parton and final-state jet resolution, with a value of $Y4JT$ smaller than the y_{cut} value to be used for jet resolution.

APACIC

The philosophy of the new approach of the APACIC MC [17] is to use ME and PS in the corresponding regimes of their reliability: matrix elements are employed to describe

the production of jets, and parton showers to model their evolution. A general algorithm to match them has been proposed and implemented in APACIC++, the PS part of the package. The algorithm is based on the paradigm above, namely to restrict the validity of the ME's for the description of particle emission to the regions of jet-production, i.e. to regions of comparably large angles and energies - or to large y_{cut} of the corresponding jet-clustering scheme. In contrast, the PS is restricted to the disjunct region of jet-evolution, i.e. small angles and low energies - or low y_{cut}, respectively. The hadronization of the partons is left to well-established schemes. At the moment, an interface to the hadronization in the Lund-string picture as implemented in PYTHIA is supplied.

The program package is designed for the modelling of multi-jet events. It is capable to produce and evaluate matrix elements for the production of up to five massive partons in QCD and at least all electroweak processes of the type $e^+e^- \to$ four fermions allowed in the Standard Model. The MEs are matched to the parton shower via an algorithm capable to deal with -in principle- any number of jets produced via the strong, weak or electromagnetic interaction on equal footing.

APACIC ++ parameters:

- *i)* $y_{cut}{}^{ini}$ Emissions of colour charged partons are restricted to resolution parameters $y_{cut} > y_{cut}{}^{ini}$.
- *ii)* $\kappa_s^{3,4,5}$ Due to the truncation of the perturbative expansion, matrix element calculations show a significant dependence on the QCD renormalization scale. APACIC++ accounts for these dependences by a scale parameter $\kappa_s^{3,4,5}$ for each n-jet configuration: $\alpha_s = \alpha_s(\kappa_s^{3,4,5} \cdot s)$, where s is the square of the center-of-mass energy of the e^+e^- system.
- *iii)* $\alpha_s(M_Z)$ The strong coupling constant is responsible for the parton shower evolution
- *iv)* cut-off PS The parton shower ends at a given energy scale, where fragmentation starts.

2.6 Extensions beyond QCD: The light gluino hypothesis

Si es que existen, he de encontrar
lenguajes de un mundo que está dormido entre las hojas de los libros.

Although experimental measurements at the highest available energy are consistent with the standard model of the strong interactions, the observed relationship of the strong coupling constant at the Z and the weak angle as well as the value of the b/τ mass ratio in relation to the top quark mass remain strong indications of a supersymmetric (SUSY) grand unification above 10^{16}GeV and a SUSY threshold for squarks and sleptons in the 0.1 to 1 TeV region. Supersymmetric phenomenology deals normally with sparticles of masses $\mathcal{O}(100)$GeV. The only exception is the light gluino with mass ≤ 1.5GeV and $3-5$GeV [19]. In this unification picture the value of the SUSY threshold is very sensitive to the highest known (two-loop) contribution to the Minimal Supersymmetric Standard Model(MSSM) β function. At the one-loop order a SUSY threshold far below 100GeV would be needed in order to fit the coupling constant measurements and such a low threshold is directly ruled out by the non-observation of squarks and sleptons in Z decay. This suggests that the three-loop results could also be important especially as the precision of the measurements at the Z and beyond improves.

As a first step in the calculation of the full three-loop β function of the MSSM, the gluino contribution to the renormalization of the strong coupling constant is taken into account. This gives the complete result in the region between the gluino mass and the squark mass which, in the light gluino scenario, extends from the low energy regime up to the Z and beyond up to the squark threshold. Then, as was seen in Section 2.3.3, the running of the strong coupling constant as a function of the scale μ is determined by the QCD β function, redefined here more conveniently as

$$\frac{d\alpha_s}{d(\ln \mu)} = -\alpha_s \beta \left(\frac{\alpha_s}{4\pi}\right) \tag{2.48}$$

where β has the perturbative expansion

$$\beta(x) = \beta_1 x + \beta_2 x^2 + \beta_3 x^3 + ... \tag{2.49}$$

Simple relations between the coefficients, e.g. $\beta_1 = b\,8\pi$, allow to go from the definition in Eq. 2.14 to the one in Eq. 2.49. Ignoring squark contributions, the one- and two-loop results in the minimally extended SUSY QCD are [20]

$$\beta_1 = \frac{22}{3} C_A - \frac{8}{3}\left(N_f T_R + \frac{N_g}{2} C_A\right) \tag{2.50}$$

$$\beta_2 = \frac{68}{3}C_A^2 - \frac{40}{3}\left(N_f T_R C_A + \frac{N_g}{2}C_A^2\right) - 8\left(N_f T_R C_F + \frac{N_g}{2}C_A^2\right) \tag{2.51}$$

where N_g is the number of gluino multiplets.

The gluino contributions to the β function coefficients as well as the additional four-jet final states can be exploited to set limits on the light gluino mass. In fact this was used in a previous ALEPH analysis [21] to exclude the existence of a gluino with mass below 6.3 GeV/c^2. In this analysis four-jet observables were used, for which only tree-level cross sections were known at that time. Similar hints were found in the analysis by Csikor and Fodor [22], based on the running of the strong coupling constant.

However, a consistent analysis looking for a hint of the existence of the light gluino, must contain the virtual gluino effects not only in the running (technically in the β function), but in all loop diagrams. As will be seen in Chapter 5, since recently calculations up to next-to-leading order exist, which will allow for a consistent analysis. The calculations are for massless quarks and a massless gluino though, preventing to set a limit on the light gluino mass.

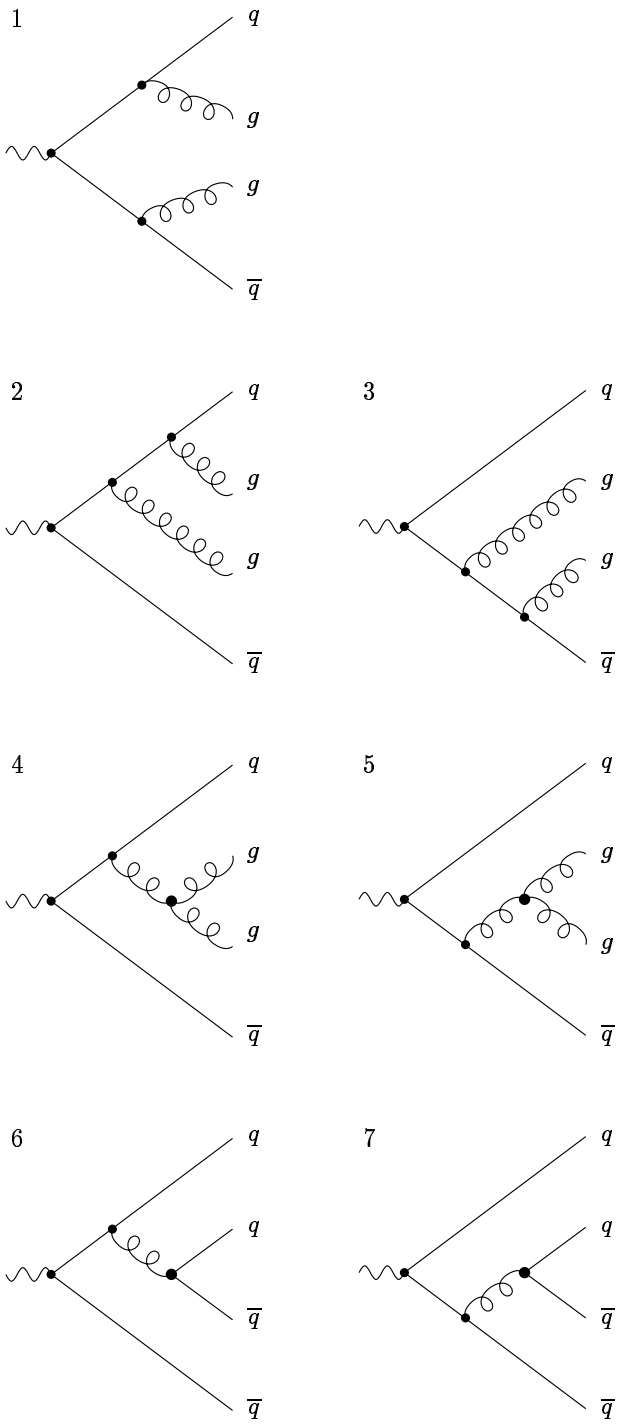

Figure 2.9: Four parton configurations.

Chapter 3

QCD predictions for Four-Jet Observables

Prometo cambiar, volverme humilde como un cristiano,
dejar de beber y aprender tu alfabeto.

3.1 Introduction

Multi-jet events at LEP have sufficiently large invariant masses to ensure that jets truly reflect the distribution of quark and gluon quanta in the femto-universe, revealing the basic couplings in the QCD Lagrangian. Four-jet events are particularly interesting for the study of QCD (see Fig. 3.1), since this theory shows its full gauge structure only in order α_s^2. They are extremely important to experimentally verify the effects of the gluon self-coupling, since the $e^+e^- \to q\bar{q}gg$ cross section dominates over the $e^+e^- \to q\bar{q}q\bar{q}$. As already seen in Chapter 2, the direct coupling between gluons is a consequence of the non-abelian nature of QCD.

The three-jet cross section is consistent with a spin-one gluon. However, one could imagine an alternative "Abelian QCD" theory, in which $SU(3)$ is replaced by $[U(1)]_3$ and the coupling is adjusted to be $\tilde{\alpha}_s = C_F\alpha_s$, so that the correct three-jet rate is obtained. It is then the four-jet rate that allows to distinguish this theory from QCD, since only a subset of the QCD Feynman diagrams contribute in the Abelian case.

The QCD cross section for four-parton production is given by

$$d\sigma^{(4)} = \left(\frac{\alpha_s}{2\pi}\right)^2 [C_F^2\mathcal{A} + C_F C_A\mathcal{B} + C_F T_R n_f\mathcal{C}] + \mathcal{O}(\alpha_s^3)\,, \tag{3.1}$$

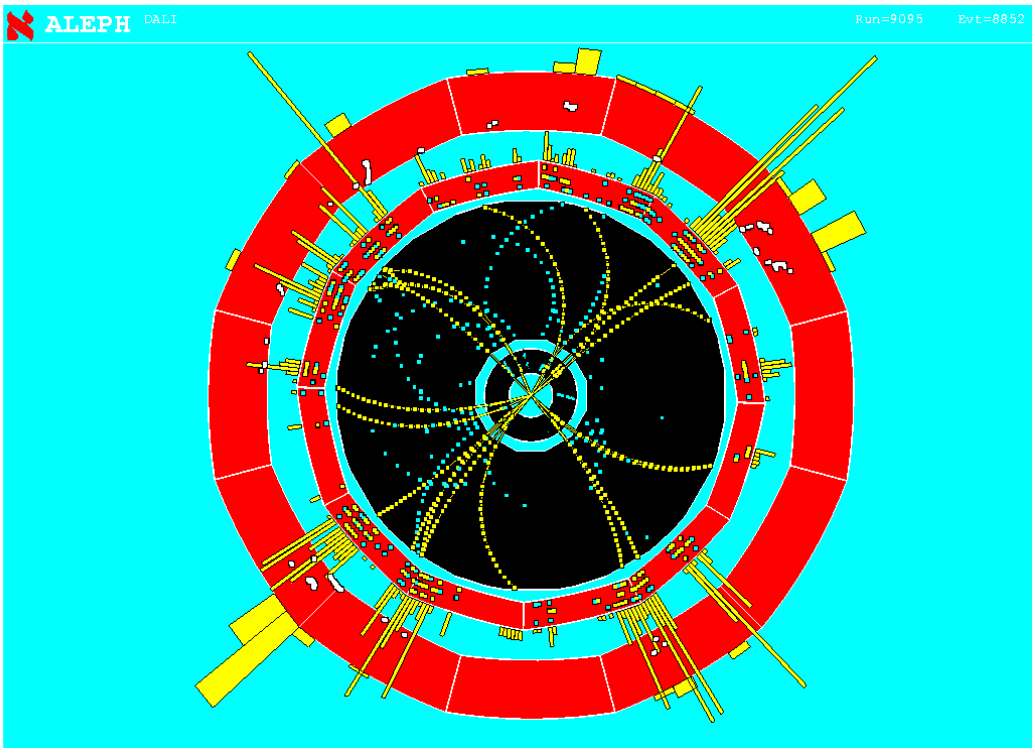

Figure 3.1: A four-jet hadronic event recorded with the ALEPH detector.

where $\mathcal{A}$, $\mathcal{B}$ and $\mathcal{C}$ are functions of the parton-parton invariant masses squared, $s_{ij} = (p_i + p_j)^2$. The last term on the right-hand side corresponds to the $q\bar{q}q\bar{q}$ final state, and is common to both the Abelian and non-Abelian theories. The first two terms correspond to the $q\bar{q}gg$ final state: the second term receives contributions from the triple-gluon vertex diagram and is absent in the Abelian theory.

With the overall couplings already fixed by the three-jet rate, the four-jet rates are therefore different in the two theories, and one could in principle discriminate between them on the basis of the overall event rate alone. In particular, the rate is much smaller for the Abelian theory, where the $q\bar{q}q\bar{q}$ final state rate is relatively more important than in QCD. The problem with this is that the magnitude of the cross section is quite sensitive to the choice of scale in the strong coupling, and this freedom would allow the overall rates to be adjusted to fit the measured rate in each case. In principle, the fraction of four-quark events would also provide a discrimination. However, it is very difficult to distinguish light-quark and gluon jets with the necessary efficiency. The only realistic possibility appears to be to tag at least three b quarks in the final state (using vertex de-

tectors or semi-leptonic decays) to estimate the fraction of $q\bar{q}q\bar{q}$ events, but the efficiency is again very low.

A much more powerful and illuminating method makes use of the different correlations among the final-state particles induced by the various contributions to the cross section. These correlations have their origin in the different angular momentum properties of the final state.

In this study both the overall four-jet rate and the so called four-jet angular correlations have been used. The four-jet rate is very sensitive to the strong coupling constant and, as the resummation of large logarithms exist, we expect its scale dependence to be heavily reduced. For the angular correlations, the sensitivity to the QCD colour factors will be exploited. In the following pages the description of these observables can be found.

3.2 Four-Jet Observables

The NLO differential cross section for a four-jet observable, O_4, can be written as,

$$\frac{1}{\sigma_0}\frac{d\sigma}{dO_4}(O_4) = \eta(\mu)^2 B_{O_4}(O_4) + \eta(\mu)^3 \left[B_{O_4}(O_4)\beta_0 \ln {x_\mu}^2 + C_{O_4}(O_4)\right] \tag{3.2}$$

with

$$\eta(\mu) = \left(\frac{\alpha_s(\mu) C_F}{2\pi}\right) \tag{3.3}$$

and where σ_0 is the Born cross section for e^+e^- annihilation into hadrons, μ is the renormalization scale, x_μ the ratio of μ with respect to the Z boson mass, and B_{O_4} and C_{O_4} are scale-independent functions. They are obtained from the integration of the fully differential massless matrix elements for e^+e^- annihilation into four-parton final states. The NLO expression is presented here, as terms at $\mathcal{O}(\alpha_s^4)$ have not yet been calculated.

For the running coupling the two-loop expression

$$\eta(\mu) = \frac{\eta(\mathrm{M_Z})}{w(\mu)}\left(1 - \frac{\beta_1'}{\beta_0'}\,\eta(\mathrm{M_Z})\frac{\ln w(\mu)}{w(\mu)}\right) \tag{3.4}$$

is used, with

$$w(\mu) = 1 - \beta_0'\,\eta(\mathrm{M_Z}) \ln\left(\frac{\mathrm{M_Z}}{\mu}\right) \quad , \tag{3.5}$$

$$\beta_0' = \frac{11}{3}x - \frac{4}{3}yN_f \quad , \quad \beta_1' = \frac{17}{3}x^2 - 2\,y\,N_f - \frac{10}{3}x\,y\,N_f \quad . \tag{3.6}$$

$x = \frac{C_A}{C_F}$ and $y = \frac{T_R}{C_F}$ are the QCD colour factor ratios. Using the expected values from $SU(3)$ for the colour factors, $C_A = 3$ and $C_F = 4/3$, together with the normalization $T_R = 1/2$, the theoretical prediction for the ratios is x=2.25 and y=0.375. β_0' and β_1' are the coefficients of the QCD β function as defined in Section 2.6 but including some factors, $\beta_0' = \beta_0/2C_F$ and $\beta_1' = \beta_1/4C_F^2$, to have as perturbative parameter $\eta(\mu)$ instead of $\alpha_s(\mu)$, and setting N_g to zero, as the light gluino hypothesis is not taken into account for the time being.

The B and C functions depend linearly and quadratically on the colour factors, as can be seen in the following expressions,

$$B_4 = B_0 + B_x\,x + B_y\,y \tag{3.7}$$

and

$$C_4 = C_0 + C_x\,x + C_y\,y + C_z\,z + C_{xx}\,x^2 + C_{xy}\,x\,y + C_{yy}\,y^2\,. \tag{3.8}$$

Such a dependence will be used, in the analyses presented in Chapter 6, for the simultaneous measurement of the strong coupling constant and the colour factors. At NLO the ratio z appears that is related to the square of a cubic Casimir operator,

$$C_3 = \sum_{a,b,c=1}^{N_A} \mathrm{Tr}\left(T^a T^b T^{\dagger c}\right) \mathrm{Tr}\left(T^{\dagger c} T^b T^a\right) \quad , \tag{3.9}$$

via $z = \frac{C_3}{N_c\,C_F^3}$.

3.2.1 Electron-Positron Annihilation Cross Section

In the previous chapter it was seen that the formation of hadrons is non-perturbative. However, a pQCD calculation of the total hadronic cross section can be obtained. The reason for this can be found when looking at the event in space-time. The electron and positron collide to form a γ or a Z of virtuality Q equal to the collision energy $\sqrt{s}$, which fluctuates into $q\bar{q}$, $q\bar{q}g$, ... By the uncertainty principle, this fluctuation occurs on a distance scale of the order $1/Q$, and if Q is large the production rate should be predicted by perturbation theory. Subsequently, the quarks and gluons form themselves into hadrons. This process, called hadronization, occurs at a much later time scale characterized by $1/\Lambda$, where Λ is the scale in α_s, i.e. the scale at which the coupling becomes strong. The interactions which change quarks and gluons into hadrons certainly modify the outgoing state, but they occur too late to modify the original probability for the event to happen,

which can therefore be calculated in perturbation theory.

The total cross section for $q\bar{q}$ production at Born level (no initial state radiation, no gluon radiation) is given by

$$\sigma_0 = \frac{12\pi\Gamma_{ee}\Gamma_{q\bar{q}}}{\mathrm{M_Z^2}\Gamma_\mathrm{Z}^2} \tag{3.10}$$

where $\mathrm{M_Z}$ is the mass of the Z boson, and Γ_{ee}, $\Gamma_{q\bar{q}}$ and Γ_Z are the partial widths for Z decay into e^+e^-, $q\bar{q}$ and the total width, respectively. Leading-order corrections, see Fig. 3.2, from pQCD to this Born cross section give

$$\sigma_\mathrm{tot} = \sigma_0\left(1+\frac{\alpha_s}{\pi}\right) = \sigma_0\left(1+\frac{3}{2}\eta\right) \tag{3.11}$$

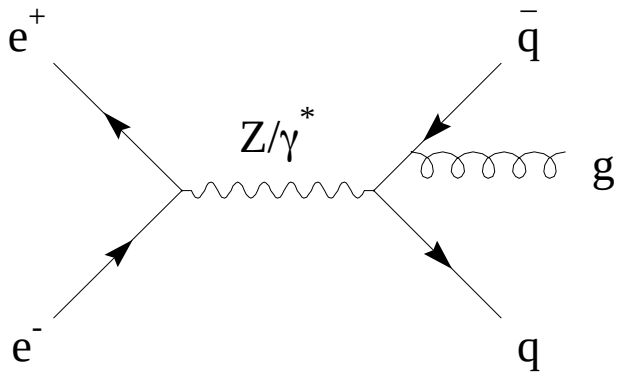

Figure 3.2: Feynman graph for the $\mathcal{O}(\alpha_s)$ correction to the Born cross section for $e^+e^- \to q\bar{q}$.

3.3 The Four-Jet Rate

The four-jet rate is used in this thesis as it is very sensitive to η (i.e. to the strong coupling constant). Following the expression in Eq. 3.2, the NLO prediction for the four-jet rate -defined as the ratio of the four-jet cross section to the total hadronic cross section- is given by:

$$\begin{aligned} R_4(\mathrm{y_{cut}}) = \frac{\sigma_{4-\mathrm{jet}}}{\sigma_\mathrm{tot}}(\mathrm{y_{cut}}) &= \eta(\mu)^2 B_4(\mathrm{y_{cut}}) \\ &+ \eta(\mu)^3\left[\beta_0\ln(x_\mu^2) + C_4(\mathrm{y_{cut}}) - \frac{3}{2}B_4(\mathrm{y_{cut}})\right], \end{aligned} \tag{3.12}$$

where y_{cut} is the clustering resolution parameter and the relation in Eq. 3.11 is used to obtain the proper normalization.

Four-jet fractions decrease very rapidly when increasing the resolution parameter, so most of the data is found at small y_{cut}. However, the fixed order perturbative prediction is not reliable for small values of y_{cut}, due to the terms ${\alpha_s}^n \ln^m y_{cut}$ that enhance the higher order corrections. The all-order resummation of the leading and next-to-leading logarithmic (NLL) contributions has to be performed. This resummation is possible with the Durham clustering algorithm [23] used in this thesis and described in Section 5.1, using the coherent branching formalism. The expression for the four-jet rate in the next-to-leading logarithmic approximation is given in [24],

$$R_4^{\mathrm{NLL}} = 2[\Delta_q(Q)]^2 \left[\left(\int_{Q_0}^{Q} dq \Gamma_q(Q,q) \Delta_g(q,Q_0) \right)^2 + \int_{Q_0}^{Q} dq \Gamma_q(Q,q) \Delta_g(q,Q_0) \times \int_{Q_0}^{q} dq' + \left(\Gamma_g(q,q') \Delta_g(q',Q_0) + \Gamma_f(q') \Delta_f(q',Q_0) \right) \right] . \tag{3.13}$$

The functions $\Delta_a(Q,Q_0)$ are the Sudakov form factors which express the probability of parton branching evolution from a scale $Q = Q_0\sqrt{y_{cut}}$ to a scale Q_0 without resolvable branching. These functions are obtained as the integrals of the emission probabilities $\Gamma_a(Q,q)$, which are:

$$\begin{aligned} \Gamma_q(Q,q) &= \frac{2C_F}{\pi} \frac{\alpha_s(q)}{q} \left[\left(1 + \frac{\alpha_s(q)}{2\pi} K \right) \ln \frac{Q}{q} - \frac{3}{4} \right] \quad , \\ \Gamma_g(Q,q) &= \frac{2C_A}{\pi} \frac{\alpha_s(q)}{q} \left[\left(1 + \frac{\alpha_s(q)}{2\pi} K \right) \ln \frac{Q}{q} - \frac{11}{12} \right] \quad , \\ \Gamma_f(Q,q) &= \frac{N_f}{3\pi} \frac{\alpha_s(q)}{q} \quad . \end{aligned} \tag{3.14}$$

The K coefficient is renormalization scheme dependent. In the $\overline{\mathrm{MS}}$ scheme it is given by [25]

$$K = C_A \left(\frac{67}{18} - \frac{\pi^2}{6} \right) - \frac{10}{9} T_R N_f \quad . \tag{3.15}$$

It was shown in reference [26] that one can obtain an improved theoretical prediction for the differential two-jet rate if the vertex probabilities are taken at next-to-leading

order, which we also consider in our analysis. Then the vertex probabilities can be written as,

$$\begin{aligned} P_{qq}(\alpha_s, z) &= C_F \left(\frac{1+z^2}{1-z} + \frac{\alpha_s}{2\pi} K \frac{2}{1-z} \right), \\ P_{gg}(\alpha_s, z) &= 2C_A \left(\frac{z}{1-z} + \frac{1-z}{z} + z(1-z) + \frac{\alpha_s}{2\pi} K \frac{2}{1-z} \right), \\ P_{gq}(\alpha_s, z) &= T_R N_f \left(z^2 + (1-z)^2 \right). \end{aligned} \tag{3.16}$$

As the Durham four-jet rate can be resummed but it does not satisfy a simple exponentiation, the only viable matching schemes are the R matching or the modified R matching [27, 28]. The one used in this study is the R matching following again reference [24]. The R-matched expression for the four-jet rate is

$$R_4^{\mathrm{R-match}} = R_4^{\mathrm{NLL}} + \left[\eta^2 \left(B_4 - B_4^{\mathrm{NLL}} \right) + \eta^3 \left(C_4 - C_4^{\mathrm{NLL}} - \frac{3}{2} \left(B_4 - B_4^{\mathrm{NLL}} \right) \right) \right] \quad . \tag{3.17}$$

In Fig. 3.3 a comparison of the predictions at different orders for the four-jet rate is shown. There we can notice that the NLO contribution is large, going from 30% to about 70% of the LO one. When the resummation is included the main difference is in the shape of the distribution. The same effect is found when the K coefficient is taken into account. As will be shown in Chapter 6, the inclusion of the K factor is needed in order to obtain a good fit of the data.

3.4 The Four-Jet Angular Correlations

Apart from the four-jet rate, four other observables have been used which are expected to be very sensitive to the colour factor ratios. These are the four-jet angular correlations:

- the Bengtsson-Zerwas angle [29]:

$$| \cos(\chi_{\mathrm{BZ}}) | = | \cos(\angle [(\vec{p}_1 \times \vec{p}_2), (\vec{p}_3 \times \vec{p}_4)]) | \tag{3.18}$$

- the Körner-Schierholtz-Willrodt angle [30]:

$$\cos(\Phi_{\mathrm{KSW}}) = \cos\left(\frac{1}{2} \left(\angle [(\vec{p}_1 \times \vec{p}_4), (\vec{p}_2 \times \vec{p}_3)] + \angle [(\vec{p}_1 \times \vec{p}_3), (\vec{p}_2 \times \vec{p}_4)] \right) \right) \tag{3.19}$$

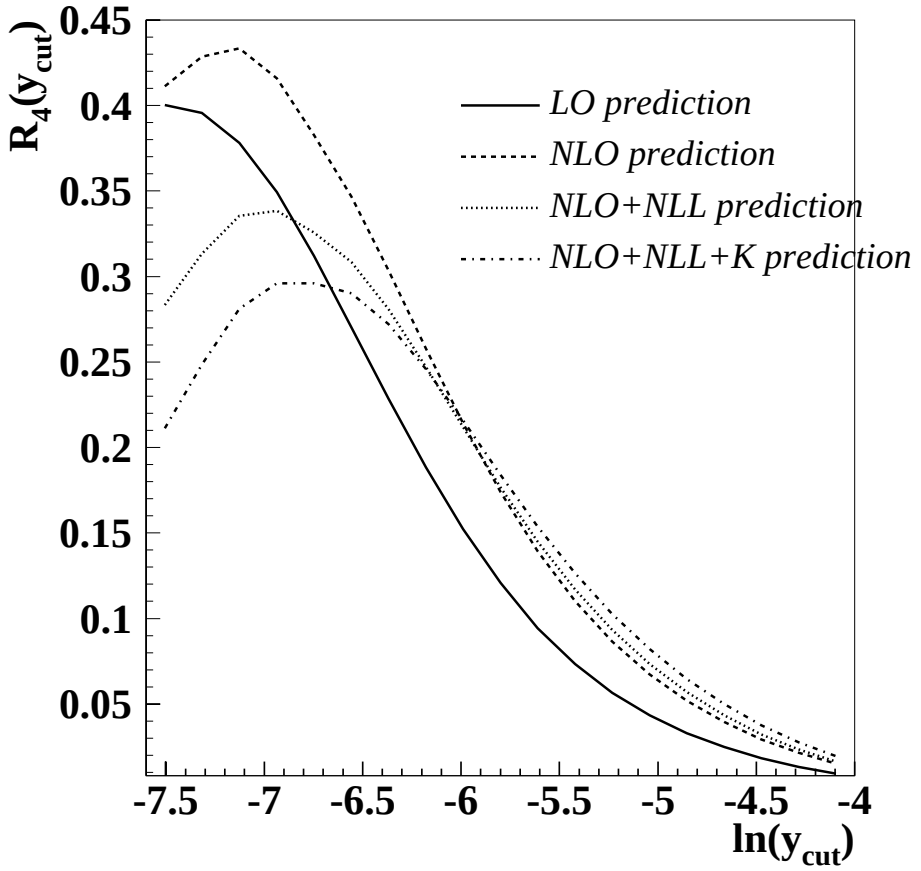

Figure 3.3: Predictions at different orders for the four-jet rate.

- the modified Nachtmann-Reiter angle [31]:

$$| \cos(\Theta_{\rm NR}) | = | \cos(\angle[(\vec{p}_1 - \vec{p}_2), (\vec{p}_3 - \vec{p}_4)]) | \tag{3.20}$$

- the angle between the two lowest energy jets [32]:

$$\cos(\alpha_{34}) \; = \; \cos(\angle[\vec{p}_3, \vec{p}_4]) \tag{3.21}$$

where p_i are the energy-ordered four-momenta ($E_1 > E_2 > E_3 > E_4$). The theoretical NLO expression for each of the angular observables will be of the form

$$\frac{1}{\sigma_0}\frac{d\sigma}{d\cos X}(\cos X) = \eta(\mu)^2 \, B_{\cos X}(\cos X) + \eta(\mu)^3 \left[B_{\cos X}(\cos X)\, \beta_0 \, \ln({x_\mu}^2) + C_{\cos X}(\cos X)\right] \tag{3.22}$$

The idea of the four-jet angular observables is to exploit the characteristic features of gluon dynamics in QCD, as opposed to abelian theories, to isolate the triple gluon vertex

in four-jet events of e^+e^- annihilation. For this, the angular correlation observables were defined to be sensitive to different types of Feynman graphs as detailed in the following paragraphs.

- Gluons radiated from q and $\bar{q}$ in $e^+e^- \to q\bar{q}g$ are linearly polarized to a high degree in the $q\bar{q}g$ final state. If χ is the angle between the final state plane and the polarization vector then we have the probability for $g \to gg \approx \left[1 + \frac{1}{9}\cos 2\chi\right]$ and for $g \to qq \approx [1 - \cos 2\chi]$. Therefore we expect the angle between the plane formed by the two lowest energetic jets (preferentially virtual gluon decays) and the plane formed by the high energy jets (mostly the primordial $q\bar{q}$) to be distributed nearly isotropically in QCD while these planes should be preferentially perpendicular in abelian theories. Even if it is very difficult to distinguish between jets induced by the primary and the secondary partons, we expect the secondary partons to be less energetic. All this takes us to the definition of the Bengtsson-Zerwas angle. See Fig. 3.4 for the difference between QCD, which has $SU(3)$ as underlying gauge group, and an abelian theory.

- In order to obtain evidence for the triple-gluon vertex the following variable was presented. $\phi_{\mathrm{KSW}} = \angle[(\mathbf{p}_1 \times \mathbf{p}_4), (\mathbf{p}_2 \times \mathbf{p}_3)]$. In theories without the triple-gluon vertex the planes orthogonal to the vectors $\mathbf{p}_1 \times \mathbf{p}_4$ and $\mathbf{p}_2 \times \mathbf{p}_3$ are uncorrelated, and because of phase space restrictions the angle Φ_{KSW} between these two planes is found around 90°, preferentially. However, if there is a triple-gluon vertex, then the pole structure of the propagator for the intermediate gluon leads to a preference for small angles between the two secondary gluons, and a correlation between the planes is induced. Because of the energy ordering, the planes turn out to be anti-parallel most of the time. The final definition found in Eq. 3.19 comes from a generalization in order to be invariant under exchange of the first and second jet, as well as of the third and fourth jet. A simplified version of the Körner-Schierholz-Willrodt angle is obtained by looking at the angle between the two lowest energetic jets. This is the definition of the fourth angular observable defined above. The angle α_{34} distinguishes between the relative contributions from double gluon radiation and gluon splitting into gluon pairs. Gluon radiation from the two primary quarks occurs more or less independently, and because of the collinear character of bremsstrahlung and the energy ordering of the four jets, large angles between the secondary partons are expected. Gluon splitting into secondary partons on the other hand will lead to rather small opening angles. In Fig. 3.5 the distributions for the same cases as in the above figure are shown for comparison.

- To find a signal for the triple gluon vertex the following kind of events are considered:

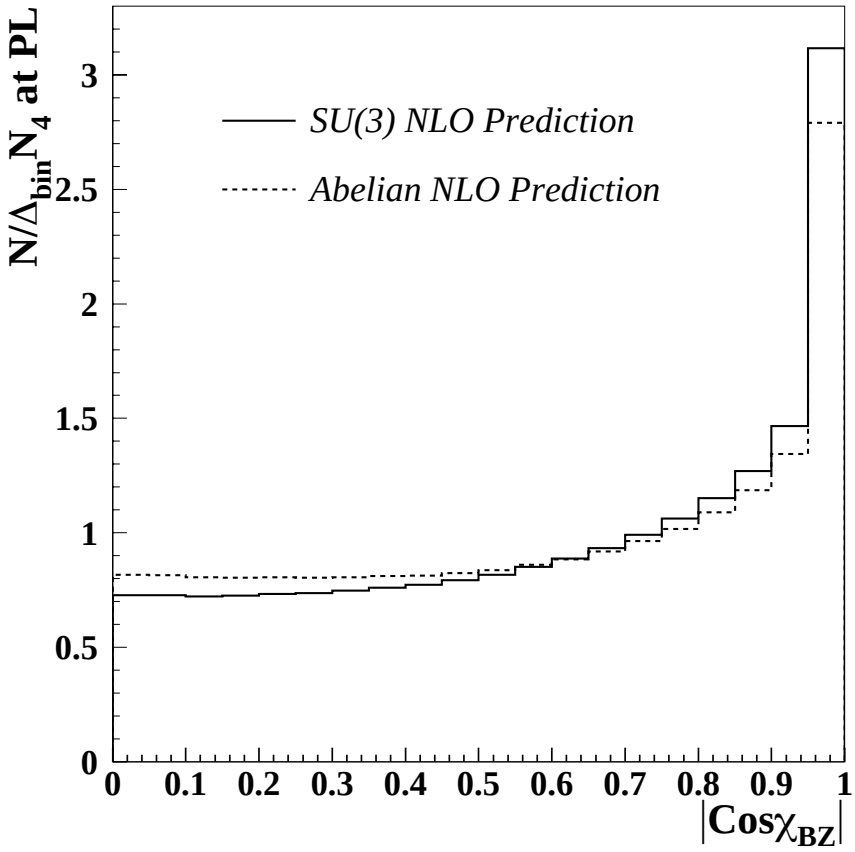

Figure 3.4: Comparison of QCD NLO predictions and abelian NLO predictions for the Bengtsson-Zerwas angle. (Durham algorithm, E-scheme, y_{cut}=0.008. See Section 5.1)

Two back-to-back jets of high energy and two back-to-back jets of much lower energy, i.e.

$$\begin{array}{ccc} \mathbf{p}_1 + \mathbf{p}_2 = 0 & & \mathbf{p}_3 + \mathbf{p}_4 = 0 \\ E_1 = E_2 & \gg & E_3 = E_4 \end{array}$$

Then $\cos\theta_{13} = (\mathbf{p}_1 \cdot \mathbf{p}_3)/|\mathbf{p}_1||\mathbf{p}_3|$, which is the angle between the axis of the high energy jets and the low energy jets is very sensitive to the presence of the triple-gluon coupling. If we concentrate on events where a virtual gluon decays either into two spin-1/2 or into two massless vector particles, the virtual gluon will have always helicity 0 with respect to the direction of the high energy jets. Therefore the helicities of the high energy quark-antiquark pair must be opposite and the pair $q\bar{q}$

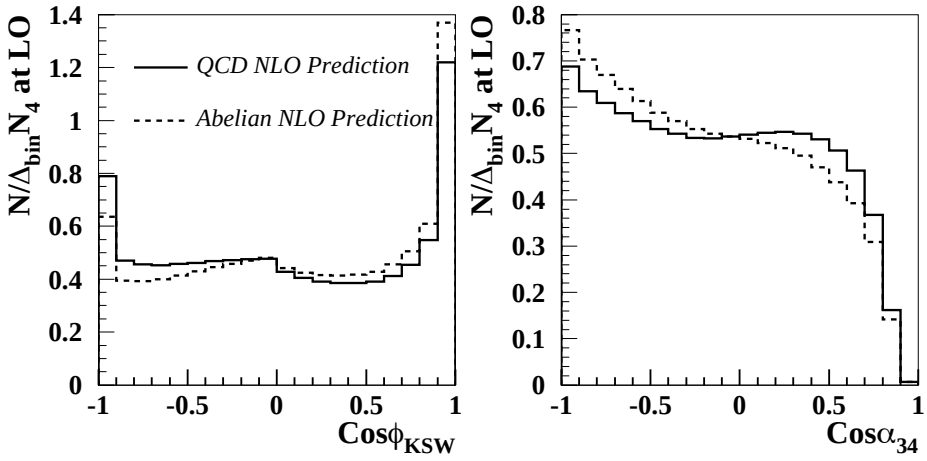

Figure 3.5: Comparison of QCD NLO predictions and abelian NLO predictions for $\cos\Phi_{\mathrm{KSW}}$ and $\cos\alpha_{34}$ (Durham algorithm, E-scheme, y_{cut}=0.008. See Section 5.1)

carries ± 1 unit of angular momentum with respect to its direction of flight. Note that a vector particle like a gluon with helicity zero in one direction has only helicity components ± 1 in any orthogonal direction. Now, if the virtual gluon decays to a massless $q\bar{q}$ pair, then the direction of these secondary partons has to be orthogonal to the primary ones. However, for a decay into two real gluons, which must have helicity ± 1, the situation is just the inverse. In summary, the following distributions are expected for different kinds of graphs:

$$\frac{d\sigma}{d\cos\theta_{13}} \propto 1 - \cos^2\theta_{13} \quad \text{for the final state } q\bar{q}q\bar{q} \tag{3.23}$$

$$\frac{d\sigma}{d\cos\theta_{13}} \propto \cos^2\theta_{13} \quad \text{for the final state } q\bar{q}gg \tag{3.24}$$

Since in QCD there are more gluon decays into two gluons than into a quark-antiquark pair, a dominance of the $\cos^2\theta_{13}$ term is expected. Of course, in reality also double bremsstrahlung diagrams occur, and $\cos\theta_{13}$ has to be restricted to values well below 1 where the perturbation theory breaks down due to collinear divergences. To solve this problem, a generalized Nachtmann-Reiter angle was proposed, Eq. 3.20, which is the one used in this thesis. Fig. 3.6 shows the comparison between a four-quark channel and a two-quark-two-gluon one.

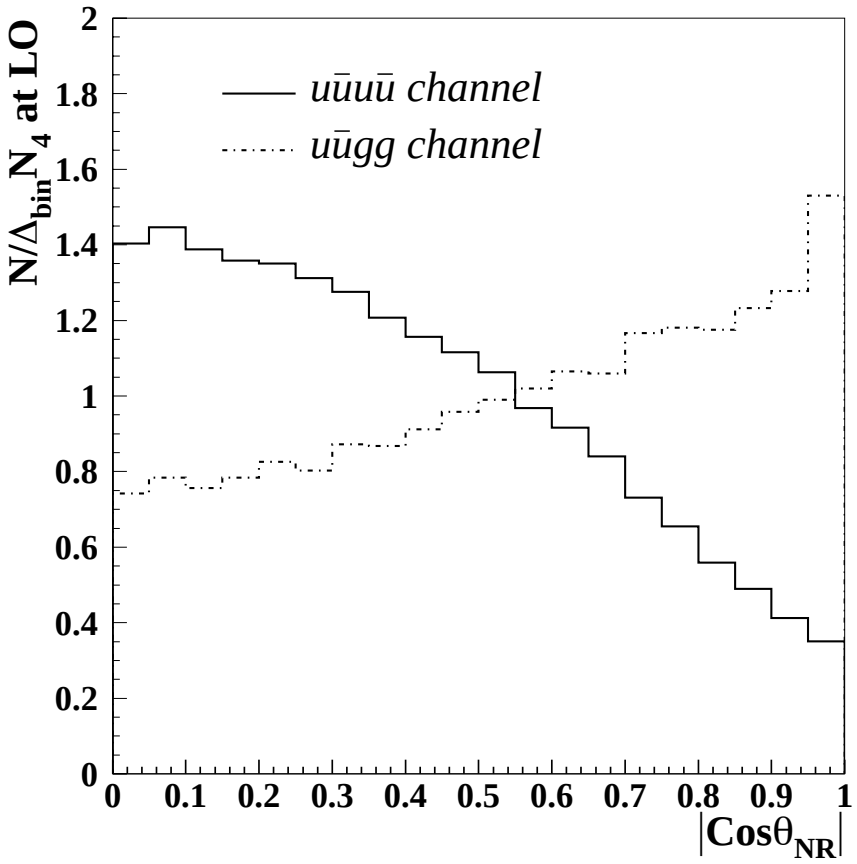

Figure 3.6: Comparison of the $|\cos\theta_{\mathrm{NR}}|$ distributions at LO between a four-quark channel and a two-quark-two-gluon channel.

3.5 Four-Jet Events and Monte Carlo implementation

The analyses of this thesis will be based on the observables described above. Thus, it is very important that four-jet events from QCD are correctly implemented in the MC programs that are widely used in phenomenological studies of hadron production at e^+e^- colliders. However, certain aspects of the four-jet production are known not to be well described by the standard "$\mathcal{O}(\alpha_s)$ ME + parton shower" MC programs. In addition, some of the observables that have shown a significant disagreement between data and MCs are the four-jet angular correlations, which will be used for the simultaneous measurement of the strong coupling constant and the colour factors.

Such discrepancies have been related to the fact that standard MCs do not provide a correct description of the spin correlations among the various partons, particularly at large jet separations. These correlations are naturally included in a full matrix element calculation, but are not necessarily included in a PS emulation for the four-jet final state. A consequence of this is that "$\mathcal{O}(\alpha_s^2)$ ME" programs, such as the option of four-parton + string fragmentation (no parton shower) implemented in PYTHIA, yielded a much better angular description of four-jet final states. However, even an "$\mathcal{O}(\alpha_s^2)$ ME + fragmentation" model, without the PS evolution, is inadequate to describe QCD four-jet production in e^+e^- collisions. The problem is that such ME models contain "ad-hoc" hadronization which is adjusted to produce a good agreement with some data, but they cannot be extrapolated to other energies. Furthermore, their description of the sub-jet structure is very poor.

Such deficiencies in the description of four-jet final states could be cured by an "$\mathcal{O}(\alpha_s^2)$ ME + PS" (plus hadronization) approach, that is now available in the commonly used MC programs, PYTHIA and HERWIG (see Section 2.5.3 for more details). There, a combination of the full angular information content of matrix elements with the detailed sub-jet structure of parton showers is tried, which should give a realistic overall description of event properties.